TRIM14 is a key regulator of the type I interferon response during *Mycobacterium tuberculosis* infection

Caitlyn T. Hoffpauir[1], Samantha L. Bell[1], Kelsi O. West[1], Tao Jing[2], Sylvia Odio-Torres[1], Jeffery S. Cox[3], A. Phillip West[1], Pingwei Li[2], Kristin L. Patrick[1], Robert O. Watson[1]

[1]Department of Microbial Pathogenesis and Immunology, Texas A&M Health Science Center, Bryan, TX 77807, USA
[2]Department of Biochemistry and Biophysics, Texas A&M University, College Station, TX 77807, USA
[3]Department of Molecular and Cell Biology, University of California Berkeley, Berkeley, California 94720, USA.

Keywords: tripartite motif, interferon stimulated genes, TRIM14, TBK1, STAT3, SOCS3, cytosolic DNA sensing, cGAS, innate immunity, IFN, bacterial pathogen, VSV

**ABSTRACT**

Tripartite motif family proteins (TRIMs) are well-characterized regulators of type I interferon (IFN) expression following cytosolic nucleic acid sensing. While many TRIMs are known to regulate innate immunity to viruses, their contribution to innate immune signaling and gene expression during bacterial infection remains largely unknown. Because *Mycobacterium tuberculosis* is a potent activator of cGAS-dependent cytosolic DNA sensing, we set out to investigate a role for TRIM proteins in regulating macrophage responses to *M. tuberculosis*. Here, we demonstrate that TRIM14, a non-canonical TRIM that lacks an E3 ligase RING domain, is a critical negative regulator of the type I IFN response in macrophages. We show TRIM14 physically interacts with both cGAS and TBK1 and that macrophages lacking TRIM14 dramatically hyperinduce interferon stimulated gene (ISG) expression following cytosolic nucleic acid agonist transfection, IFN-β treatment, and *M. tuberculosis* infection. Consistent with loss of negative regulation in these cells, *Trim14* knockout (KO) macrophages have more phospho-Ser754 STAT3 relative to phospho-727 and fail to upregulate the STAT3 target *Socs3* (Suppressor of Cytokine Signaling 3), which is required to turn off type I IFN signaling. These data support a model whereby TRIM14 acts as a scaffold between TBK1 and STAT3 to promote phosphorylation of STAT3 at Ser727 and promote negative regulation of ISG expression. Remarkably, *Trim14* KO macrophages are significantly better than control cells at limiting *M. tuberculosis* replication. Collectively, these data reveal a previously unappreciated role for TRIM proteins in regulating type I IFN responses in response to cytosolic DNA sensing and *M. tuberculosis* infection.

## INTRODUCTION

*Mycobacterium tuberculosis*, arguably the world's most successful pathogen, elicits a carefully orchestrated innate immune response allowing it to survive and replicate in humans for decades. Infection of macrophages with *M. tuberculosis* sets off a number of pathogen sensing cascades, most notably those downstream of TLR2 (1), which senses bacterial lipoproteins and glycolipids, and cGAS, which senses bacterial DNA in the host cytosol (2-4). cGAS-dependent DNA sensing during *M. tuberculosis* infection elicits two distinct and somewhat paradoxical responses: targeting of a population of bacilli for destruction in lysosomes via ubiquitin-mediated selective autophagy, and activation of a type I interferon (IFN) gene expression program, which is inadequate at controlling bacterial pathogenesis *in vivo*. Because both selective autophagy and type I IFN have been repeatedly shown in animal and human studies to be hugely important in dictating *M. tuberculosis* infection outcomes (5-7), there is a critical need to elucidate the molecular mechanisms that drive their activation.

Many members of the TRIM family of proteins have emerged as important regulators of a variety of innate immune responses (5-7). Defined on the basis of their tripartite domain architecture, TRIMs generally encode a RING domain with E3 ligase activity, a B-box that is a zinc-binding domain with a RING-like fold (8), and a coil-coiled domain that mediates dimer/multimerization and protein-protein interactions (9). In addition to these domains, TRIMs encode a highly variable C-terminal domain. Early studies of TRIMs identified a role for the retroviral restriction factor TRIM5 in inhibiting HIV infection in Old-world monkeys (10). Since those initial discoveries, a variety of TRIMs have been shown to play critical roles in antiviral innate immunity through polyubiquitination of key molecules in DNA and RNA sensing cascades, including MDA5 by TRIM13, TRIM40, and TRIM65 (14-17), RIG-I by TRIM25 and TRIM40 (11, 12), and TBK1 by TRIM11 and TRIM23 (13). We are just beginning to appreciate the complex and dynamic network of regulatory factors, including TRIMs, that employ cells to upregulate and downregulate innate immune signaling and gene expression (14).

Recent work has shown that cytosolic nucleic acid sensing pathways are also engaged during infection with a variety of intracellular bacterial pathogens, including *M. tuberculosis*, *Legionella pnuemophila*, *Listeria monocytogenes*, *Francisella novicida*, and *Chlamydia trachomatis* (15). Some of these pathogens, like *M. tuberculosis and C. trachomatis*, have been shown to activate cGAS via bacterial dsDNA (2, 16), while others like *L. monocytogenes* directly activate STING by secreting cyclic di-AMP (17). It is becoming increasingly clear that activation of the cytosolic nucleic acid sensing pathways provides some benefit to intracellular bacterial pathogens, and thus the ability to engage with and manipulate regulatory molecules like TRIM proteins is likely a conserved bacterial adaptation. *Salmonella* Typhimurium has been shown to secrete SopA, an effector molecule which targets TRIM56 and TRIM65 to stimulate innate immune signaling through RIG-I and MDA5 (18, 19). Likewise, TRIM8 has been shown to regulate inflammatory gene expression downstream of TLR3 and TLR4 during *Salmonella* Typhimurium-

induced septic shock (20). In addition, ablation of TRIM72 in alveolar macrophages enhances phagocytosis and clearance of *Psuedomonas aeruginosa* (21).

Realizing the huge potential for TRIM proteins in tipping the balance between pro- and anti-bacterial innate immune outcomes, we decided to study TRIMs during *M. tuberculosis* infection, specifically a non-canonical TRIM family member: TRIM14. Like most TRIMs, TRIM14 encodes a coiled-coil, a B-box, and a C-terminal PRY/SPRY domain, but curiously it lacks the E3 ligase RING domain, likely rendering it unable to catalyze ubiquitination of proteins. Consistent with it being a major player in antiviral innate immunity, TRIM14 has been shown to directly influence replication of several RNA viruses including influenza A via interaction with the viral NP protein (22), hepatitis B via interaction with HBx (23), and hepatitis C via interaction with NS5A (24). In the context of RNA sensing, TRIM14 has been shown to localize to mitochondria and interact with the antiviral signaling adapter MAVS (25). More recently, TRIM14 has been shown to promote cGAS stability by recruiting the deubiquitinase USP14 and preventing autophagosomal targeting of cGAS (26).

Here, we demonstrate that TRIM14 is a crucial negative regulator of *Ifnb* and ISG expression during macrophage infection with *M. tuberculosis*. TRIM14 is recruited to the *M. tuberculosis* phagosome and can directly interact with both cGAS and the DNA sensing kinase TBK1. Deletion of *Trim14* leads to dramatic hyperinduction of *Ifnb* and ISGs in response to several cytosolic nucleic acid agonists, including *M. tuberculosis*. In *Trim14* KO macrophages we observe preferential phosphorylation of the transcription factor STAT3 at Ser754 and lack of association of STAT3 with the chromatin loci of target genes like the crucial negative regulator of type I IFN signaling, *Socs3*. Such data argue that TRIM14 acts as a negative regulator of cytosolic DNA sensing through bringing TBK1 and STAT3 together to promote phosphorylation of STAT3 at Ser727. *Trim14* KO macrophages were remarkably efficient at limiting *M. tuberculosis* replication but permissive for vesicular stomatitis virus (VSV), consistent with previous reports (26). Collectively, this work highlights a previously unappreciated role for TRIM14 in controlling the innate immune response *M. tuberculosis* and suggest a complex role for TRIM14 in regulating type I IFN gene expression.

## RESULTS

### TRIM14 is a player in *M. tuberculosis* infection of macrophages

Having previously described a crucial role for cGAS-dependent cytosolic DNA sensing in activating selective autophagy and type I IFN expression during *M. tuberculosis* infection (2), we set out to identify novel regulators of these pathways. Therefore, we infected bone marrow derived macrophages (BMDMs) with wild type *M. tuberculosis* (Erdman strain) and the Tn5370::Rv3877/EccD1 mutant (27), which lacks the functional virulence-associated ESX-1 secretion system (ΔESX-1) that has previously been shown to be required for activation of

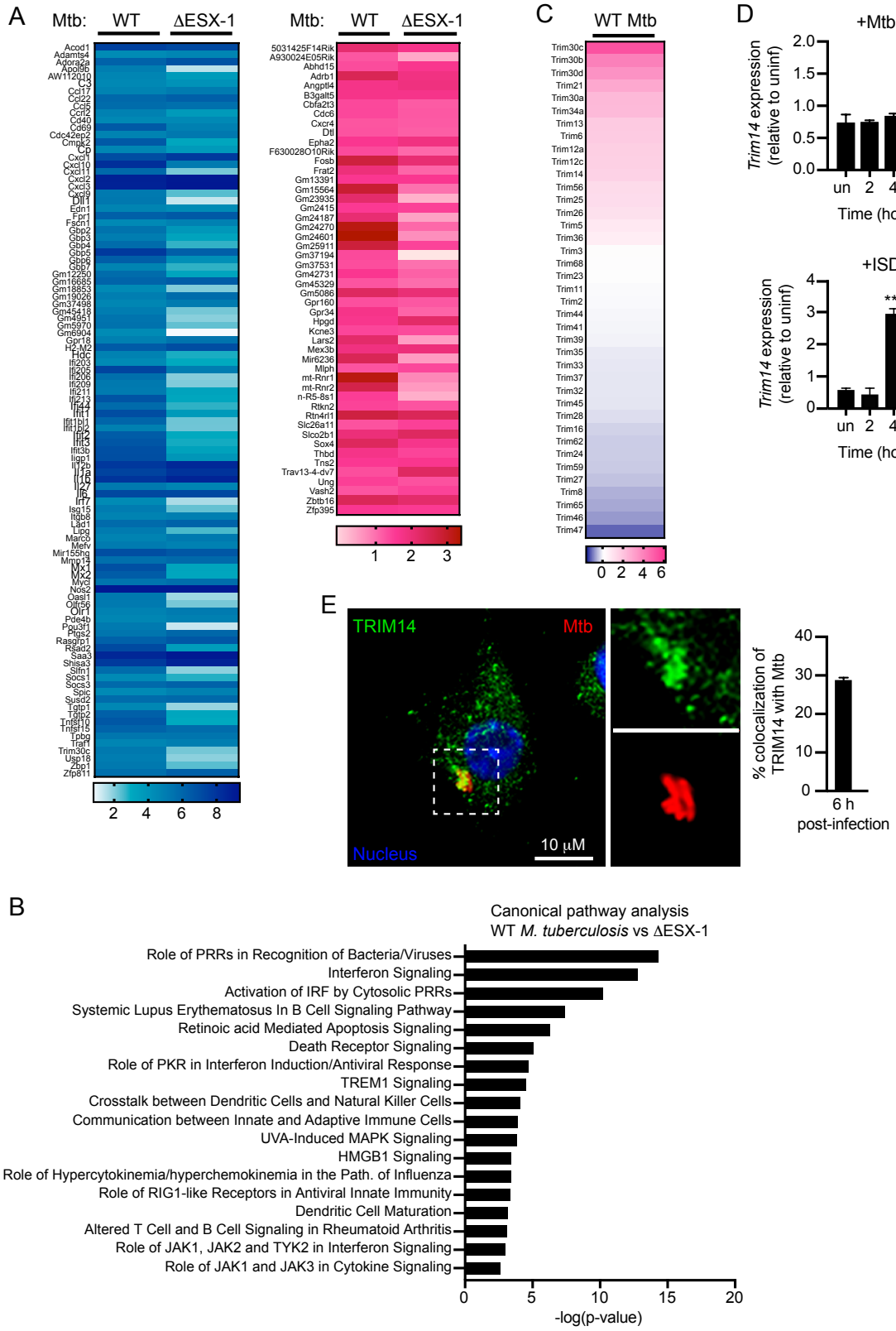


**Figure 1. TRIMs are players in the innate immune response to *M. tuberculosis.*** (A) Heatmap of significant ($p < 0.05$) gene expression differences ($\log_2$ fold-change over uninfected) in BMDMs infected with WT vs ΔESX-1 *M. tuberculosis* (Mtb). (B) IPA software analysis of cellular pathways enriched for differentially expressed genes in BMDMs infected with WT vs ΔESX-1 *M. tuberculosis*. (C) Heatmap of significant ($p < 0.05$) gene expression differences ($\log_2$ fold-change) in TRIM family genes in BMDMS infected with WT vs ΔESX-1 *M. tuberculosis*. (D) RT-qPCR of fold-change in *Trim14* transcripts in BMDMs stimulated with ISD or infected with WT *M. tuberculosis*. (E) RAW 264.7 cells infected with mCherry *M. tuberculosis* for 6 hours and immunostained for TRIM14. Statistical significance was determined using two-tailed students' t test. *$p < 0.05$, **$p < 0.01$, ***$p < 0.001$. See also Figure S1 and Table S1.

cytosolic DNA sensing (28, 29). We performed RNA-seq at an established key innate immune time point of 4 hours post-infection (Table S1). Consistent with previous microarray data (29), we observed dramatic induction of pro-inflammatory cytokines (*Il6*, *Il1b*) and antimicrobial molecules like *Nos2* in macrophages infected with both wild-type and ΔESX-1 *M. tuberculosis* (Fig. 1A). Since permeability of the *M. tuberculosis* phagosome is required for activation of cytosolic DNA sensing (29), we measured significantly lower levels of ISGs in ΔESX-1-infected BMDMs vs. those infected with wild-type bacilli (Fig. 1A). Ingenuity pathway analysis (IPA) further demonstrated ESX-1-dependent differential expression of type I IFN response genes (Fig. 1B), with "Inferferon signaling" and "Activation of IRF by Cytosolic PRRs" being the major pathways differentially expressed in wild-type vs. ΔESX-1-infected macrophages. In analyzing these lists of upregulated genes, we noticed that several of them belonged to the TRIM family, consistent with TRIMs generally being ISGs (Fig. 1C) (30). Because so little is known about how TRIM proteins regulate anti-bacterial immunity, we wanted to understand how these proteins influence cGAS-dependent innate immune outcomes during *M. tuberculosis* infection.

Based on its recent characterization as a regulator of cGAS stability (26), we decided to investigate a role for TRIM14 during *M. tuberculosis* infection. RT-qPCR analysis confirmed that *Trim14* expression was upregulated after *M. tuberculosis* infection of BMDMs (Fig. 1D), and transfection of BMDMs with dsDNA (ISD) (31) recapitulated *Trim14* induction, although with faster kinetics (Fig. 1E). This suggests that *Trim14* upregulation during *M. tuberculosis* infection occurs downstream of cytosolic DNA sensing. We next asked whether TRIM14 associated with the *M. tuberculosis* phagosome using immunofluorescence microscopy and an antibody against endogenous TRIM14. We observed about 30% of *M. tuberculosis* phagosomes stained positive for TRIM14, reminiscent of the number of phagosomes we have previously shown to be positive for ubiquitin (Ub) and LC3, two markers of selective autophagy (Fig. 1E) (32). Together, these data strongly suggest that TRIM14 contributes to the macrophage response to *M. tuberculosis*.

**TRIM14 interacts with components of the DNA sensing pathway.**

Based on its recruitment to the *M. tuberculosis* phagosome, we hypothesized that TRIM14 may interact with one or more components of the cytosolic DNA sensing pathway, which we have previously observed to co-localized with *M. tuberculosis* (Fig. 2A and (2)). We transfected epitope-tagged versions of mouse TRIM14 (3xFLAG-TRIM14) and the major components of the DNA sensing pathway (mouse HA-cGAS, HA-STING, and HA-TBK1) into murine embryonic fibroblasts (MEFs). Following 24 hours of expression, cells were fixed, and co-immunostained. Consistent with a previous report (24), we observed that TRIM14 co-localized with cGAS but not STING (Fig. 2B). Intriguingly, we also observed substantial co-localization between 3xFLAG-TRIM14 and HA-TBK1, suggesting that TRIM14 may influence multiple nodes of the cytosolic DNA sensing pathway.

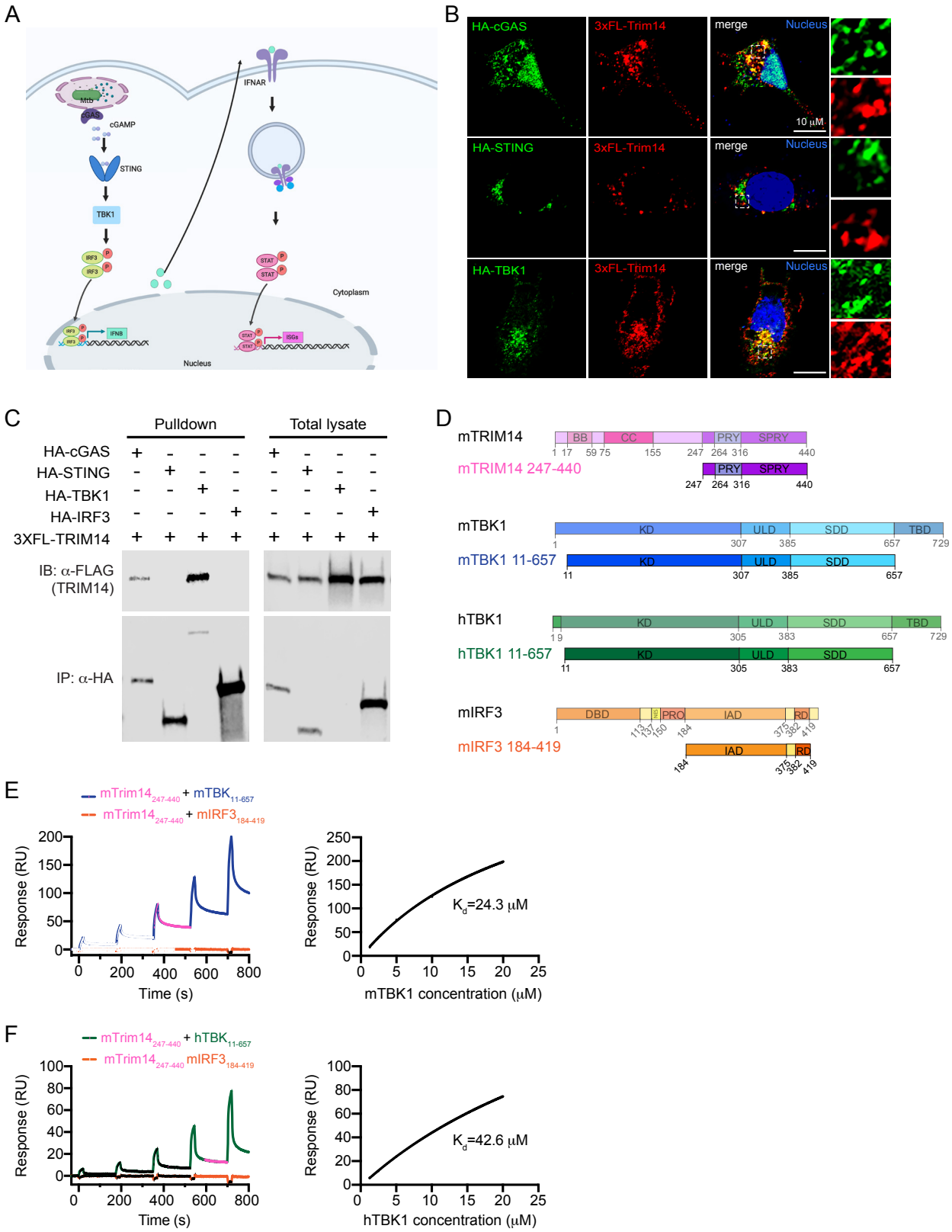


**Figure 2. TRIM14 interacts with both cGAS and TBK1 in the DNA sensing pathway.** (A) Model of DNA sensing pathway during *M. tuberculosis* infection (B) Immunofluorescence microscopy of MEFs expressing 3xFLAG-TRIM14 with HA-cGAS , HA-STING , or HA-TBK1 co-stained with α-HA and α-Flag antibodies (C) Western blot analysis of co-immunoprecipitation of 3xFLAG-TRIM14 coexpressed with HA-cGAS , HA-STING , HA-TBK1, or HA-IRF3 in HEK293T cells. Blot is representative of >3 independent biological replicates. (D) Diagram of mTRIM14, mTBK1, hTBK1, mIRF3 gene domains and truncations used in surface plasmon resonance (SPR) studies. (E) Equilibrium binding study of mTRIM14 and mTBK1 by SPR. mIRF3 was used as a negative control. Dissociation constant ($K_d$= 24.3μM) was derived by fitting of the equilibrium binding data to a one-site binding model. (F) As in (E) but with mTRIM14 and hTBK1. Dissociation constant ($K_d$= 42.6μM) was derived by fitting of the equilibrium binding data to a one-site binding model. See also Figure S2.

To further characterize this previously unappreciated association between TRIM14 and TBK1, we co-expressed 3xFLAG-TRIM14 with the major players of DNA sensing, HA-cGAS, HA-STING, HA-TBK1, and HA-IRF3 in HEK293T cells, immunopurified each of the DNA sensing pathway components, and probed for interaction with TRIM14 by western blot. Consistent with our immunofluorescence microscopy data, we found that TRIM14 co-immunoprecipitated with both cGAS and TBK1 but not STING or IRF3 (Fig. 2C). To determine whether this interaction was direct, we performed surface plasmon resonance (SPR) experiments. Briefly, full length and truncated versions of mouse TRIM14 (residues 247-440), human cGAS (residues 157-522), and mouse and human TBK1 (residues 11-657) were expressed using a baculovirus system. A portion of mouse IRF3 (residues 184-419) served as the negative control (Fig. 2D). Each of these protein truncations had previously been shown to be stably expressed at high levels and remain soluble when generated in insect cells (33-35). Equilibrium binding studies measured a binding affinity of 24.3 μM for binding between mTRIM14 and mTBK1 (Fig. 2E) and a slightly lower affinity of 42.6 μM for mouse TRIM14 and human TBK1 (Fig. 2F). We also measured an affinity of 25.8 μM between human cGAS and mouse TRIM14 (Fig. S2). No binding was measured between mTRIM14 and mIRF3. Combined, these *in vivo* and *in vitro* biochemical data argue strongly for a direct interaction between TRIM14 and TBK1.

**Loss of TRIM14 leads to type I IFN and ISG hyperinduction during *M. tuberculosis* infection**

To investigate the function of TRIM14 in the type I IFN response, we first tested how knockdown of *Trim14* affects *Ifnb* gene expression. *Trim14* knock down (KD) macrophages were generated by transducing RAW264.7 cells with lentiviral shRNA constructs designed to target the 3'UTR of *Trim14* or a control scramble shRNA (SCR). RT-qPCR analysis confirmed ~50% and 70% knockdown of *Trim14* using two different shRNA constructs (KD1 and KD2 respectively) (Fig. 3A). *Trim14* KD and control RAW264.7 cells were either infected with *M. tuberculosis* or transfected with ISD and *Ifnb* transcripts were measured at 4 hours. In both experiments, we observed lower levels of *Ifnb* transcript induction in *Trim14* KD cell lines compared to the SCR control (Fig. 3B and 3C), supporting a role for TRIM14 in the DNA sensing pathway. Since residual levels of TRIM14 protein in knockdown cell lines could potentially complicate interpretation of phenotypes, we generated *Trim14* knockouts (KO) using CRISPR-Cas9. Briefly, *Trim14*-specific guide RNAs (gRNAs) were designed to target exon 1 and a GFP-specific gRNA was designed as a negative control. Two clones with a stop codon introduced early in exon 1 were identified and chosen for subsequent experimentation (Fig. 3D). Knockout of *Trim14* was confirmed by western blot using an antibody against the endogenous protein (Fig. 3E) and by anti-TRIM14 immunofluorescence of control and *Trim14* KO cells (Fig. 3E and S3).

In order to test how genetic ablation of *Trim14* affects cytosolic DNA sensing, *Trim14* KO and control macrophages were infected with wild type *M. tuberculosis* and RNA was collected over a 24 hour time-course of infection. Surprisingly, while we again measured lower *Ifnb*

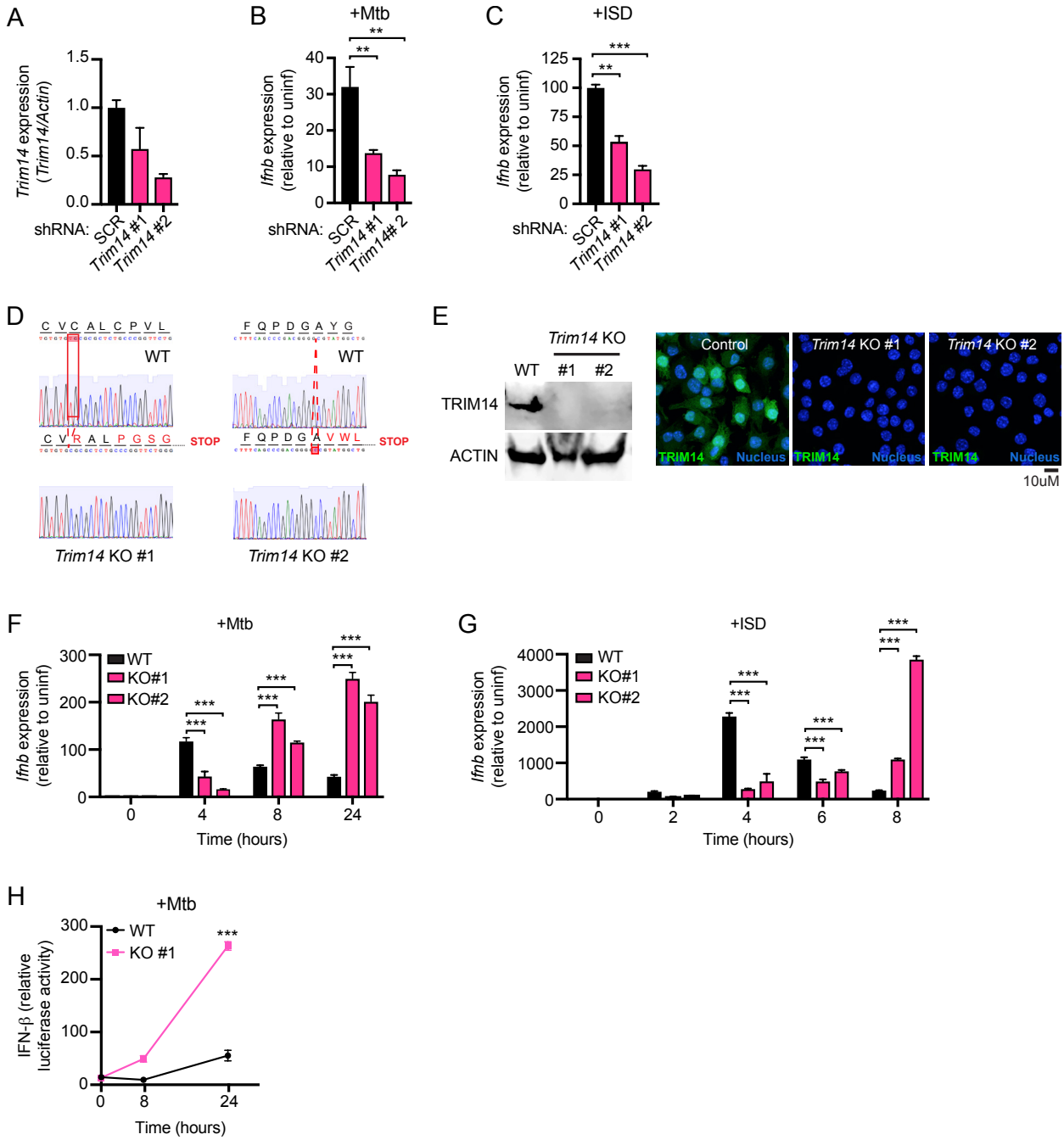


**Figure 3. Loss of Trim14 leads to hyperinduction of *Ifnb* in response to *M. tuberculosis* and cytosolic DNA.** (A) RT-qPCR of *Trim14* transcript in RAW 264.7 macrophages stably expressing shRNA to either SCR control or *Trim14*. (B) RT-qPCR of *Ifnb* transcript in RAW 264.7 macrophages stably expressing shRNA to either SCR control or *Trim14* infected with *M. tuberculosis* at 4h post infection. (C) RT-qPCR of *Ifnb* transcript in RAW 264.7 macrophages stably expressing shRNA to either SCR control or TRIM14 transfected with 1μg ISD at 4h post infection. (D) Sequencing chromatogram depicting mutations in *Trim14* gRNA CRISPR/Cas9 RAW 264.7 macrophages compared to GFP gRNA control (WT). (E) Western blot analysis and immunofluorescence microscopy of *Trim14* in WT vs *Trim14* KO RAW 264.7 macrophages using an anti-TRIM14 antibody. (F) RT-qPCR of *Ifnb* transcripts in WT and *Trim14* KO RAW 264.7 macrophages infected with *M. tuberculosis* at specified times after infection. (G) RT-qPCR of *Ifnb* transcripts in WT and *Trim14* KO RAW 264.7 macrophages treated with ISD at specified times after treatment. (H) ISRE reporter cells expressing luciferase with relative light units measured as a readout for IFN-β protein. Statistical significance was determined using two-tailed students' t test. *p < 0.05, **p < 0.01, ***p < 0.001.

expression at 4 hours post-infection, we observed a dramatic hyperinduction of *Ifnb* at later infection time points in the absence of TRIM14 (Fig. 3F). To determine the contribution of cytosolic DNA sensing to this phenotype, we transfected *Trim14* KO and control RAW 264.7 cells with ISD and again found significantly higher induction of I *Ifnb* in the absence of TRIM14 at 8 hours and 24 hours post-transfection (Fig. 3G). To verify that the transcript changes we observed translated to differences in protein levels, we used Interferon Stimulated Response Element (ISRE) luciferase reporter cells to analyze IFN-β protein secretion in supernatants from cells 8- and 24-hours post-*M. tuberculosis* infection. Using relative light units as a proxy for IFN-β, we again observed hyperinduction of IFN-β in the absence of TRIM14 (Fig. 3H). These data suggest that the major phenotype associated with *Trim14* ablation in RAW264.7 macrophages is loss of negative regulation following cytosolic DNA detection.

Having observed higher *Ifnb* transcript and protein levels in *Trim14* KO RAW 264.7 cells, we predicted that these cells also hyperinduce ISGs following treatment with innate immune agonists that either stimulate IRF3 signaling downstream of cGAS or STAT signaling downstream of Interferon alpha/beta receptor (IFNAR). RT-qPCR analysis of RNA recovered over a time-course of either *M. tuberculosis* infection or ISD transfection showed hyper induction of *Ifit1*, *Isg15*, and *Irf7* (Fig. 4A and B). High levels of *Ifit1*, *Isg15*, and *Irf7* were also observed when cells were transfected with 1μg poly (I:C), a potent agonist of RNA sensing via RIG-I (Fig. 4C) or treated with recombinant IFNβ directly (Fig. 4D). Collectively, these results demonstrate that TRIM14 is needed to turn on *Ifnb*/ISG expression at early time points and turn it off at later time points, arguing for a model whereby TRIM14 regulates cytosolic DNA sensing at two different nodes in the pathway.

**TRIM14 regulates STAT3 activation through TBK1**

Since we detected *in vivo* and *in vitro* interactions between TRIM14 and TBK1, we hypothesized that TRIM14-dependent misregulation of TBK1 activity could drive hyperinduction of *Ifnb* and ISGs. TBK1 is a prolific innate immune kinase with many known targets. We predicted that one TBK1 substrate, STAT3 (Signal transducer and activator of transcription 3) could be involved since it is one of the major transcription factors responsible for the negative regulation of the type I IFN response (36, 37). Indeed, co-immunoprecipitation experiments with STAT3 and TRIM14 revealed STAT3 binds to Trim14 (Fig. 5A) and STAT3 and TBK1 have been previously reported to interact (38).

Previous studies have demonstrated that TBK1 can directly phosphorylate STAT3 at Ser727 and Ser754 upon cytosolic DNA sensing (45). Phosphorylation of STAT3 at Ser754 inhibits STAT3's ability to interact with target genes, while phosphorylation of STAT3 at Ser727 activates STAT3 to interact with target genes (39). Based on interactions between TBK1, TRIM14 and STAT3, we next asked whether knocking out *Trim14* impacts TBK1's ability to phosphorylate

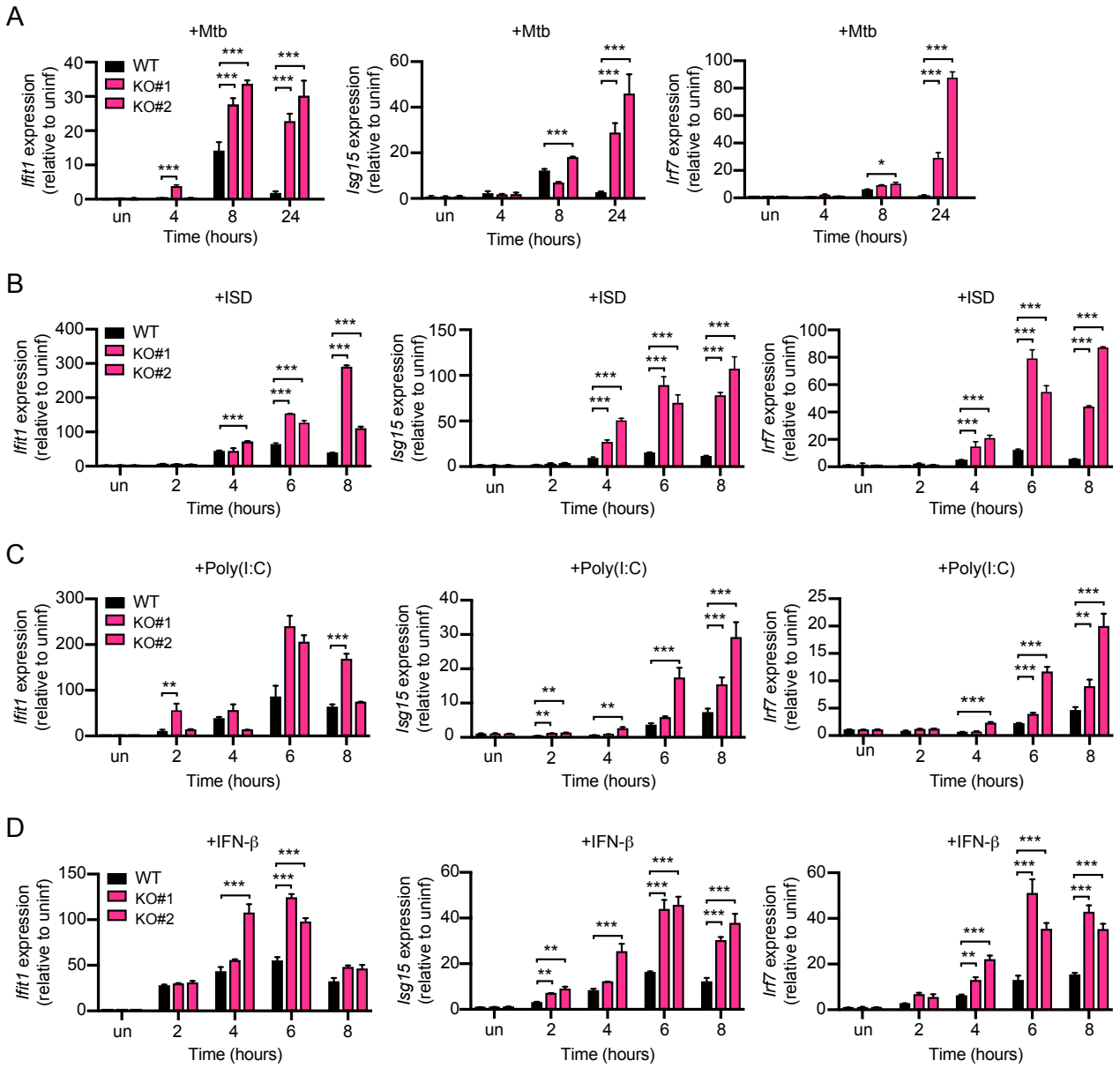


**Figure 4. Loss of TRIM14 leads to hyperinduction of ISGs in response to multiple innate immune agonists.** (A) RT-qPCR of *Ifit*, *Isg15*, *Irf7* transcripts in WT and *Trim14* KO RAW 264.7 macrophages infected with *M. tuberculosis* at specified times after infection. (B) RT-qPCR of *Ifit*, *Isg15*, *Irf7* transcripts in WT and *Trim14* KO RAW 264.7 macrophages transfected with 1μg ISD. (C) As in (B) but with poly(I:C) transfection. (D) As in (B) but with IFNβ treatment (200 IU). Statistical significance was determined using two-tailed students' t test. *p < 0.05, **p < 0.01, ***p < 0.001.

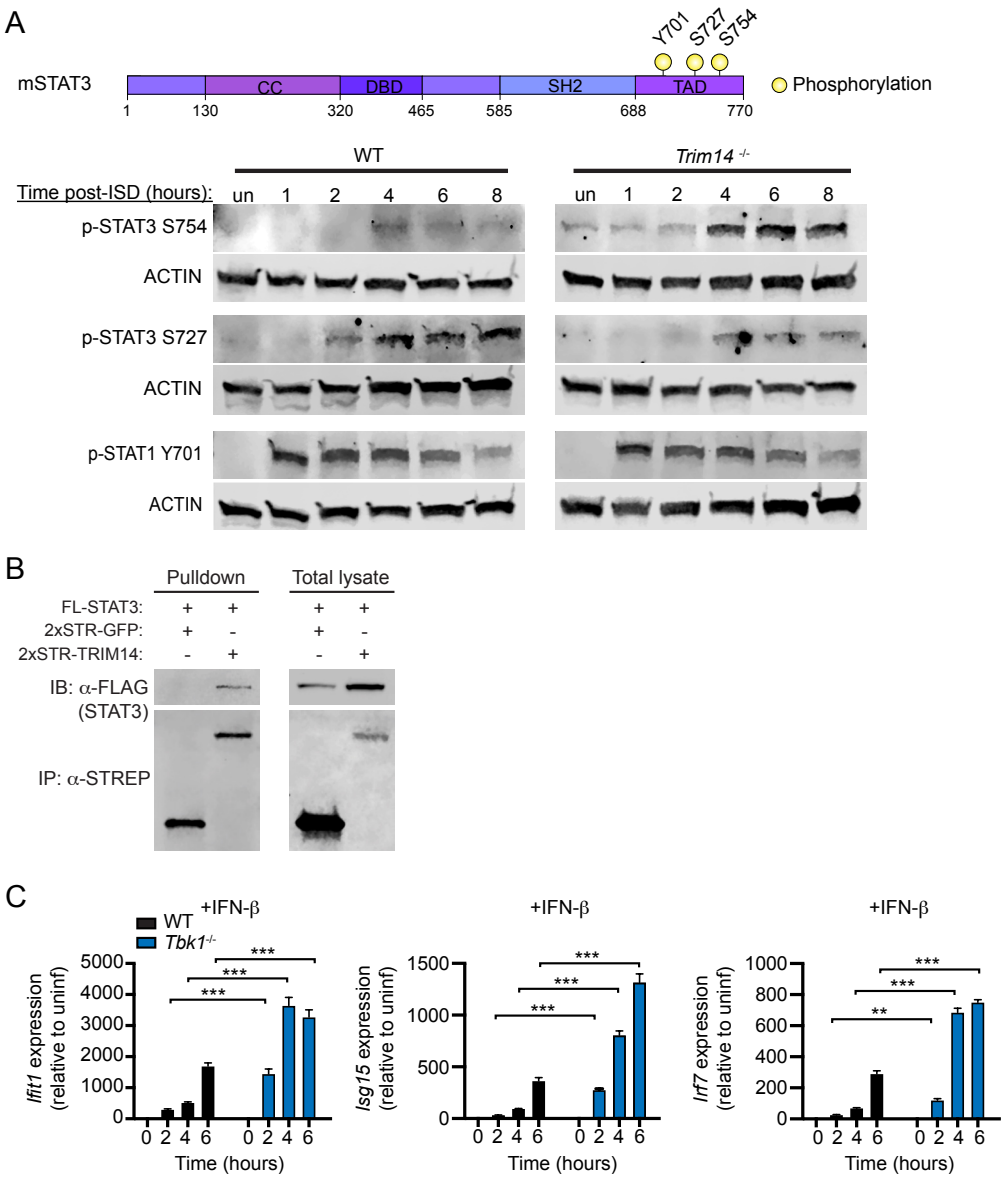


**Figure 5. Loss of TRIM14 promotes inhibitory phosphorylation of STAT3 at Ser754.** (A) Co-immunoprecipitation and western blot analysis of HEK293T cells co-transfected with FLAG-STAT3 and HA-TRIM14. (B) Immunoblot of phospho-STAT3 Ser754, phospho-STAT3 Ser727, and phospho-STAT1 Y701 in WT and *Trim14* KO RAW 264.7 macrophages at 1, 2, 4, 6, 8h post-ISD transfection. ACTIN is shown as a loading control. (C) RT-qPCR of *Ifit*, *Isg15*, *Irf7* transcripts in WT and *Tbk1* KO BMDMs treated with IFN-β. Western blots are representative of >3 independent biological replicates. Statistical significance was determined using two-tailed students' t test. *p < 0.05, **p < 0.01, ***p < 0.001. See also Figure S5.

STAT3. We transfected control and *Trim14* KO cells with ISD and analyzed STAT3 phosphorylation at Ser727 and Ser754 by immunoblot over a time-course. We observed substantially more phospho-Ser754 STAT3 and significantly less phospho-Ser727 STAT3 in the absence of TRIM14, although phosphorylation at Y701 was unchanged (Fig. 5B). These data suggest a role for TRIM14 in influencing TBK1's preference to phosphorylate particular serine residues in the transactivation domain of STAT3.

To test whether loss of TBK1 phenocopies loss of TRIM14, we harvested BMDMs from *Tbk1*$^{-/-}$/*Tnfr*$^{-/-}$ mice (40, 41) and transfected them with ISD. Remarkably, despite the fact that TBK1 phosphorylation of IRF3 is required for *Ifnb* expression downstream of cytosolic DNA sensing (42, 43), the major phenotype we observed in *Tbk1*$^{-/-}$/*Tnfr*$^{-/-}$ macrophages following ISD transfection is ISG hyperinduction (Fig. 5C), suggesting that TBK1 plays a crucial yet mostly unappreciated role in diminishing the type I IFN response.

**TRIM14 is required for STAT3-dependent transcription of *Socs3*, a negative regulator of the type I IFN response**

Because an uncontrolled type I IFN response is deleterious to the host, cells have evolved multiple mechanisms to dampen type I IFN gene expression following pathogen sensing or IFNAR engagement. The hyperinduction of *Ifnb* and ISGs we measured in *Trim14* KO macrophages is consistent with a loss of negative regulation; therefore, we hypothesized that expression of one or more negative regulators would be lower in *Trim14* KO cells. Inhibition of JAK1-STAT signaling is a well-characterized mechanism through which type I IFN signaling is downregulated (44). SOCS (Suppressor of cytokine signaling) family proteins are ISGs that dampen type I IFN responses by interfering with JAK1 kinase activity and limiting STAT signaling (37). USP18 (Ubiquitin Specific Peptidase 18) has similarly been shown to inhibit type I IFN expression by blocking interaction between JAK1 and the IFNAR2 subunit (45). To test whether *Trim14* KO cells were defective in expressing negative regulators of type I IFN, we measured *Socs3*, *Socs1*, and *Usp18* transcripts in control and *Trim14* KO RAW 264.7 cells infected with *M. tuberculosis* or transfected with ISD. Similar to all ISGs we examined in these studies, *Socs1* and *Usp18* were hyperinduced in *Trim14* KO macrophages. However, we observed a dramatic defect in *Socs3* induction, suggesting that one or more *Socs3* transcription factors were impacted by loss of *Trim14* (Figure 6A and 6B).

Previous reports have shown that *Socs3* is a target of STAT3 (46, 47). Having measured increased phosphorylation at the "inhibitory" Ser754 residue of STAT3 in *Trim14* KO macrophages, we hypothesized that lack of *Socs3* induction could be due to the inability of phospho-Ser754 STAT3 to bind at the *Socs3* promoter. To test this, we transfected control and *Trim14* KO cells with ISD and performed chromatin immunoprecipitation (ChIP) at 0h, 1h, and 6h following treatment. Consistent with low *Socs3* transcription, we detected significantly less recruitment of STAT3 to the *Socs3* genomic locus at both 1 and 6 hours after ISD transfection

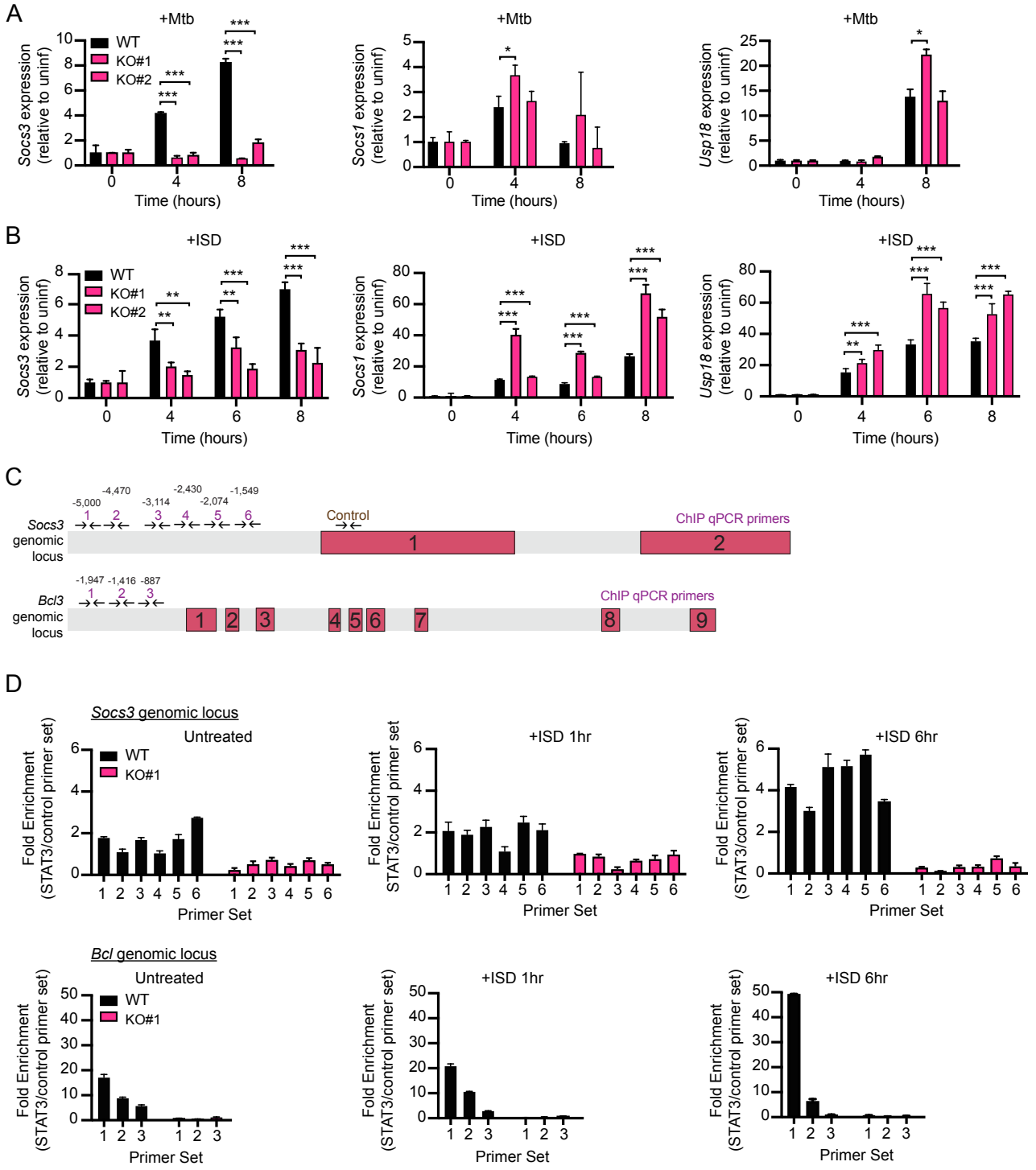


**Figure 6. *Trim14* KO macrophages fail to induce expression of the negative regulator of the type I IFN response, Socs3.** (A) RT-qPCR of *Socs3*, *Socs1*, and *Usp18* transcripts in WT and *Trim14* KO RAW 264.7 macrophages infected with *M. tuberculosis* at specified times after treatment. (B) RT-qPCR of *Socs3*, *Socs1*, and *Usp18* transcripts in WT and *Trim14* KO RAW 264.7 macrophages treated with ISD at specified times after treatment. (C) qPCR primers designed to tile *Socs3* and *Bcl3* genes for chromatin immunoprecipitation experiments (D) ChIP-qPCR of 3xFLAG-STAT3 associated genomic DNA from the *Socs3* and *Bcl3* loci in WT and *Trim14* KO RAW 264.7 macrophages transfected with 1 μg ISD. Statistical significance was determined using two-tailed students' t-test. *p < 0.05, **p < 0.01, ***p < 0.001. See also Figure S6.

(Fig. 6D). We also detected lower STAT3 recruitment to other target genes, including *Bcl3* and *Cxcl9* (Fig. 6D and S6), suggesting that loss of TRIM14 broadly impacts STAT3's ability to translocate to the nucleus and/or associate with DNA. From these data, we conclude that lack of *Socs3* induction may contribute to ISG hyperinduction in the absence of TRIM14.

**Loss of TRIM14 impacts the ability of macrophages to control infection**

Having demonstrated an important role for TRIM14 in regulating the type I IFN response, we set out to investigate how loss of TRIM14 impacts cell-autonomous innate immune responses to viral and intracellular bacterial infection. To test how loss of TRIM14 impacted survival and replication of *M. tuberculosis*, we infected control and *Trim14* KO macrophages with M. *tuberculosis* expressing the *luxBCADE* operon from *Vibrio harveyi* (48) and bacterial replication was quantified as a measure of luminescence over a 72 hour time course (48, 49). Remarkably, we observed a dramatic inhibition of *M. tuberculosis* replication in *Trim14* KO macrophages (Figure 7A). Importantly, this lack of *M. tuberculosis* replication did not correspond to loss of cells, as infected monolayers remained completely intact at the 72 hour time point (Fig. S7).

We next infected control and *Trim14* KO RAW 264.7 cells with VSV, an enveloped RNA virus that elicits rapid and robust gene expression changes in macrophages (Kandasamy et al., 2016). VSV replication was measured by RT-qPCR of VSV-G and VSV-M over a 12 hour time-course. Although uptake of virus, as inferred by viral genome measurements at the 1 hour time point was very similar between the two genotypes, we observed a dramatic hyperreplication of VSV in *Trim14* KO macrophages (Fig. 7B). Consistent with results from poly(I:C) RNA transfection (Fig. 4C), we again measured significantly higher *Ifnb* and ISG expression in *Trim14* KO macrophages (Figure 7D). Although this result initially appeared to be at odds with hyperreplication of VSV, it is consistent with low basal levels of *Ifnb* and ISGs that persist in resting macrophages lacking TRIM14 (Figure 7C). We propose that *Trim14* KO cells are more susceptible to very early replication of VSV due to destabilization of cGAS and low intrinsic type I IFN expression. Because *Trim14* KO macrophages are not primed to combat viral infection, even later hyperinduction of ISGs cannot compensate once viral replication has "taken off" in the absence of TRIM14. As *M. tuberculosis* replicates very slowly (~24 hour doubling time), we propose that unlike VSV, whose replication can be influenced by low resting ISGs in *Trim14* KO cells, *M. tuberculosis* replication is restricted by hyperinduction of ISGs that dominate after 4 hours of infection.

**DISCUSSION**

Potent inflammatory innate immune responses like induction of type I IFN require tight temporal control. Here, we demonstrate a previously unappreciated role for TRIM14 in downregulating *Ifnb* and ISG expression following cytosolic innate immune danger signals. We

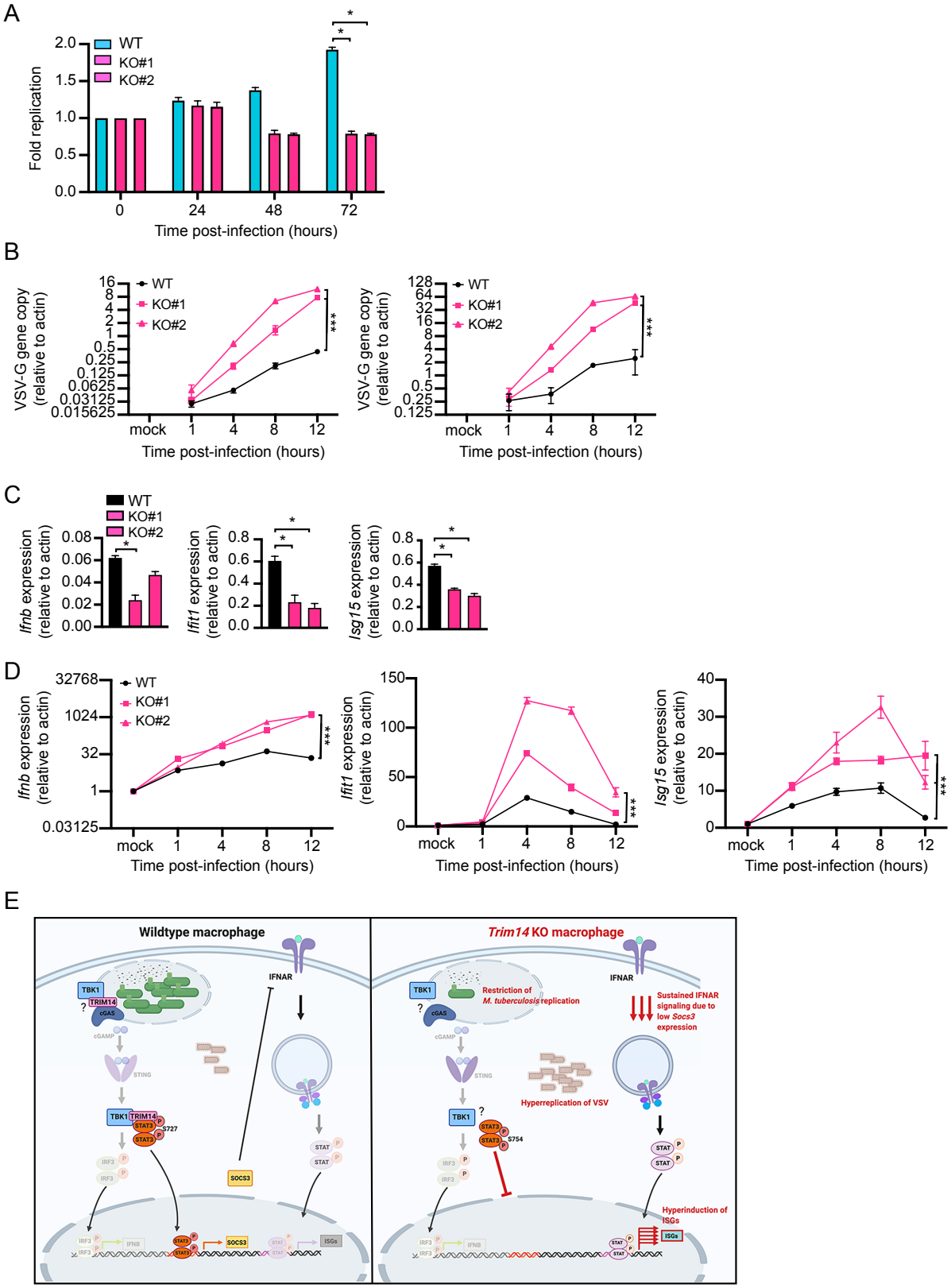


**Figure 7. *Trim14* KO macrophages restrict *M. tuberculosis* replication but fail to control VSV replication.** (A) Fold replication of Mtb *luxBCADE* in WT and *Trim14* KO RAW 264.7 macrophages. (B) Viral replication in WT and *Trim14* KO RAW 264.7 macrophages infected with VSV (MOI=1.0 or Mock infected) at 1, 4, 8, and 12 h post-infection. (C) RT-qPCR of *Ifnb*, *Ifit1*, and *Isg15* transcript levels in mock infected WT and *Trim14* KO RAW 264.7 macrophages. (D) RT-qPCR of *Ifnb*, *Ifit1*, and *Isg15* transcript levels in WT and *Trim14* KO RAW 264.7 macrophages at 1, 4, 8, and 12 h post-infection with VSV (MOI=1). (E) Proposed model of TRIM14's dual roles in regulating cytosolic DNA sensing. TRIM14/cGAS interaction is required to inhibit proteosomal degradation of cGAS and TRIM14/TBK1 interaction is required to promote TBK1-dependent phosphorylation of STAT3 at Ser727 and activate transcription of negative regulators of the type I IFN response like *Socs3*. See also Figure S7.

provide strong evidence that TRIM14 can directly interact with TBK1 and that loss of TRIM14 results in preferential phosphorylation of STAT3 at Ser754. Together, these data support a model whereby TRIM14 acts as a scaffold between TBK1 and STAT3, promoting TBK1-dependent phosphorylation of STAT3 at Ser727 and transcriptional activation of negative regulators of JAK/STAT signaling like SOCS3 (Figure 7E). Consistent with a role for STAT3 in primarily turning off type I IFN responses, *STAT3* KO mouse embryonic fibroblasts (MEFs) and BMDMS also hyperinduce ISGs following viral infection (36).

There is mounting evidence that a complex network of post-translational modifications regulates STAT3's ability to dimerize, translocate to the nucleus, and/or bind DNA (37). Acetylation of STAT3 at lysine 685 and phosphorylation of tyrosine 705 have both been shown to increase the protein's ability to bind DNA and translocate to the nucleus (50, 51). Likewise, phosphorylation at Ser727 promotes transcriptional activation by STAT3, while phosphorylation at Ser754 inhibits cytosolic DNA-induced STAT3 transcriptional activity and reduces expression of STAT3 target genes (39). We propose that in the context of DNA sensing, TBK1-dependent phosphorylation of STAT3 acts as a control point for ramping up or down the STAT3 transcriptional regulon, and TRIM14 can tip this balance. It is curious that these two modifications have dramatic opposing effects on STAT3 activity, as they both occur in the transactivation domain. Structural studies are needed to shed light on how modulation of TBK1/STAT3 interactions by TRIM14 promote Ser727 phosphorylation over Ser754 phosphorylation. It is possible that the presence of TRIM14 makes one site more accessible either directly through interactions with STAT3 or by modulating interactions with other binding partners that influence availability of the two serine residues. As STAT3 is hugely important not only for controlling inflammatory responses during infection but also for regulating embryogenesis, cancer mestastasis, and apoptosis, there is a critical need to understanding how factors like TRIM14 can regulate its activation.

A previous study demonstrated a similar role for TRIM14 in controlling VSV replication but reported that *TRIM14* KO macrophages had lower ISG expression compared to wild-type (26). The authors ascribe these phenotypes to TRIM14's role in promoting cGAS stabilization and provide evidence that loss of TRIM14 allows for cGAS degradation via the E3 ligase USP14 that targets cGAS to p62-dependent selective autophagy. We also observed lower *Ifnb* in response to *M. tuberculosis* and ISD transfection for our earliest measurements (4 hours for *M. tuberculosis* infection; 2, 4, and 6 hours for ISD transfection) (Fig. 3A, F, and G), but the phenotype of *Trim14* KO macrophages shifts to hyperinduction at later time points. It is not entirely clear what accounts for the discrepancies in our data, although notably, our analysis focuses almost exclusively on early time points following viral infection or innate immune activation (1-12 hours) as opposed to the 12-24 hours Chen *et al.* focused on during which cell death resulting from high viral titers may complicate measurement and interpretation of transcript abundance. Taking the conclusions from both studies into account, it seems likely that TRIM14 plays a dual role in type I IFN regulation

whereby it interacts with cGAS to promote type I IFN expression and with TBK1/STAT3 to dampen it (Fig. 7E). Future work will need to investigate the precise spatiotemporal distribution of cGAS/TRIM14- and TBK1/TRIM14/STAT3-containing complexes over the course of type I IFN induction and resolution. It will also be important to investigate how and when TRIM14 itself is post-translationally modified. Recent work from Jia *et al.*, provides evidence for RNF125-mediated polyubiquitination and proteosomal degradation of a mitochondrially-associated population of TRIM14 during viral infection (52). This post-translational modification and others could be critical for controlling whether TRIM14 influences type I IFN responses at the level of cGAS or TBK1/STAT3.

Our finding that *Trim14* KO macrophages are better at controlling *M. tuberculosis* replication is quite surprising. We have previously shown that knocking out cGAS renders macrophages more permissive to *M. tuberculosis* infection, likely through loss of selective autophagy downstream of cytosolic DNA sensing (2). Therefore, it is unlikely that TRIM14's early negative regulation of IFNB through its contribution to cGAS stability can explain the dramatic *M. tuberculosis* replication restriction we observed. It is possible that overexpression of guanylate binding proteins (GBPs), which have been previously reported to be required for cell-intrinsic control of mycobacterial replication (53), could inhibit *M. tuberculosis* growth in TRIM14 KO macrophages. Alternatively, loss of TRIM14 could promote anti-*M. tuberculosis* selective autophagy perhaps by freeing up a population of TBK1 to associate with the phagosome to help recruit selective autophagy machinery and LC3. Additional experiments designed to investigate what proteins TRIM14 interacts with on *M. tuberculosis* phagosome and how loss of TRIM14 impacts maturation of the autophagosome will provide important insights into how TRIM14 controls *M. tuberculosis* replication and shed light on how we may be able to manipulate TRIM14 as a tuberculosis therapeutic.

**ACKNOWLEDGMENTS**

We would like the acknowledge Monica Britton at the University of California, Davis DNA Technologies & Expression Analysis Core Library for her help with the RNA-seq analysis. We would also like to acknowledge the members of the Patrick and Watson labs for help with editing the manuscript, their valuable discussions, and critical feedback.

## MATERIALS AND METHODS

Cell Culture

RAW 264.7 macrophages, HEK293T, MEF, and LentiX cells were cultured at 37°C with 5% $CO_2$. Cell culture medium was comprised of High glucose, sodium pyruvate, Dulbecco's modified Eagle medium (Thermo Fisher) with 10% FBS (Sigma Aldrich) 0.5% HEPES (Thermo Fisher).

Co-immunoprecipitations

1.8 x $10^6$ HEK293T cells in a 10cm plate were transfected with 1-10 µg of pDEST 3xFlag TRIM14, pDEST HA cGAS, pDEST HA STING, pDEST HA TBK1, pDEST HA IRF3, pDEST Flag STAT3, or pDEST HA TRIM14 using PolyJet In Vitro DNA Transfection Reagent. Cells were harvested in PBS+0.5M EDTA 24 hours post-transfection and pellets were lysed on ice with lysis buffer (50 mM Tris HCl pH 7.4, 150 mM NaCl, 1 mM EDTA, 0.075% NP-40) containing protease inhibitor (Pierce A32955). Strep-tactin superflow plus beads (Qiagen) were washed using buffer containing 5% 1M Tris at pH 7.4, 3% NaCl, and 0.2% 0.5M EDTA. 1000 µl of the cleared lysate was added to the beads and inverted for 2 hr at 4°C. Beads were then washed 4 times with wash buffer (50 mM Tris HCl pH 7.4 150 mM NaCl 0.5M EDTA, 0.05% NP-40) and eluted using 1x Biotin. Whole cell lysate inputs and elutions were boiled in 4x SDS loading buffer with 10% 2-mercapethanol. Proteins were run on SDS-PAGE gels (Bio-Rad) and then transferred to nitrocellulose membrane (GE Healthcare). Membranes were blocked in TBS (Odyssey Blocking buffer Li-COR) for 1 hour and incubated with primary antibody overnight at 4°C. LI-COR secondary was used (IR Dye CW 680 goat anti-rabbit, IR Dye CW 680 goat anti-rat 680, IR Dye CW800 goat anti-mouse (LI-COR)) and developed with the Odyssey Fc by LI-COR. Immunoprecipitation experiment were also performed as stated above but with Pierce Anti-HA agarose (Thermo 26181). Beads were eluted three times at room temperature for 15 min each using Influenza Hemagglutinin (HA) peptide (Sigma Aldrich I2149).

Western Blot analysis

Protein samples were run on Any kD Mini-PROTEAN TGX precast protein gels (BioRad) and transferred to 0.45 µm nitrocellulose membranes (GE Healthcare). Membranes were incubated in the primary antibody of interest overnight and washed three times with TBS-Tween 20. Membranes were then incubated in secondary antibody for 1 hour and imaged using LI-COR Odyssey FC Imaging System. Primary antibodies used in this study: mouse monoclonal α-FLAG M2 antibody (Sigma-Aldrich, F3165), α-HA high affinity rat monoclonal antibody (Roche; 3F10), α-strep (Genscript A00626), α-phospho-Stat3 (Ser727) (Cell Signaling #9134), α-phospho-Stat3 (Ser754) (Cell Signaling #98543), α-Stat3 (124H6) Mouse mAb (Cell Signaling #9139), α-phospho-Stat1 (Tyr701) (58D6) Rabbit mAb #9167, α-TRIM14 G-15 (Santa Cruz sc79761), α-TRIM14 (Aviva ARP34737), and α-mouse monoclonal Beta-Actin (Abcam, #6276). Secondary

antibodies used in this study: IR Dye CW 680 goat anti-rabbit, IR Dye CW 680 goat anti-rat 680, IR Dye CW800 goat anti-mouse (LI-COR), Alexfluor-488 anti-rabbit, Alexfluor-597 anti-rat, and Alexafluo-647 anti-mouse secondary antibodies for immunofluorescence (LI-COR).

Construction of sgRNA/Cas9 LentiCRISPR and viral transduction

Guide RNAs targeting the first exon of Trim14 were designed using the Broad online tool (https://portals.broadinstitute.org/gpp/public/analysis-tools/sgrna-design). The top five hits were used to design five guide RNA constructs that were cloned into Lenti CRISPR vector (Puromycin) at the BsmB1 site. Constructs were sequenced and verified. Plasmids were then transfected into Lenti-X cells with PAX2 and VSVG packing plasmids. Virus was collected 24 and 48 hours post-transfection and stored at -80°C. RAW264.7 cells stably expressing Cas9 were then transduced with virus and selected using puromycin for 72 hours. Cells were then clonally selected using serial dilutions and clones were selected from wells calculated to contain a single cell. To verify the knockout, genomic DNA was collected from cells and the first exon of TRIM14 was amplified using PCR. This reaction was sent for sequencing to verify the mutation.

Generation of shRNA-expressing stable cell lines

To generate knockdown RAW 264.7 macrophages, plasmids of scramble non-targeting shRNA constructs and TRIM14 shRNA constructs targeted towards the 3' UTR of TRIM14 were transfected into Lenti-X cells with PAX2 and VSVG packing plasmids. Virus was collected 24 and 48 hours post-transfection and stored at -80°C. RAW264.7 cells were then transduced with virus and selected using hygromycin at 10mg/ml (Invitrogen) to select for cells containing the shRNA plasmid.

Macrophage stimulation

RAW 264.7, CRISPR/Cas9 RAW 264.7, or shRNA RAW 264.7 macrophages were plated on 12-well tissue-culture treated plates at a density of $3 \times 10^5$ cells/well and allowed to grow overnight. Cells were then transfected with 1 µg/ml ISD or 1 µg/ml poly(I:C) with lipofectamine or treated with 200units recombinant mouse IFNB (pbl assay science Cat#12400-1).

*M. tuberculosis* Infection

Low passaged lab stocks of each Mtb strain (Erdman strain WT, Erdman *luxBCADE*, or Erdman m-Cherry) were thawed for each experiment to ensure virulence was preserved. *M. tuberculosis* was cultured in roller bottles at 37°C in Middlebrook 7H9 broth (BD Biosciences) supplemented with 10% OADC, 0.5% glycerol, and 0.1% Tween-80. All work with Mtb was performed under Biosafety Level 3 (BSL3) containment using procedures approved by the Texas A&M University Institutional Biosafety Committee. To prepare the inoculum, bacteria grown to log phase (OD 0.6-0.8) were spun at low speed (500g) to remove clumps and then pelleted and washed with PBS

twice. Resuspended bacteria were briefly sonicated and spun at low speed once again to further remove clumps. The bacteria were diluted in DMEM + 10% horse serum and added to cells at an MOI of 10 for RNA and cytokine analysis and MOI of 1 for microscopy studies. Cells were spun with bacteria for 10 min at 1000 x g to synchronize infection, washed twice with PBS, and then incubated in fresh media. RAW 264.7 or CRISPR/Cas9 RAW 264.7 macrophages were plated on 12-well tissue-culture treated plates at a density of $3\times10^5$ cells/well and allowed to grow overnight. Where applicable, RNA was harvested from infected cells using 0.5 ml Trizol reagent at each time point.

*M. tuberculosis* survival/replication

RAW 264.7 or CRISPR/Cas9 RAW 264.7 macrophages were plated on 12-well tissue-culture treated plates at a density of 2.5 $x10^5$ cells per well. Luminescence was read for Mtb *luxBCADE* by lysing in 400ul 0.5% Triton-X and splitting into two wells of a 96 well white plate and using the luminescence feature of the INFINITE 200 PRO by TECAN at 0, 24, 48, and 72 hours post infection.

RNA isolation and qPCR analysis

In order to analyze transcripts, cells were harvested in Trizol at the specified time points and RNA was isolated using Direct-zol RNA Miniprep kits (Zymo Research) with 1 hour DNase treatment. cDNA was synthesized with iScript cDNA Synthesis Kit (Bio-Rad). cDNA was diluted to 1:20 for each sample. A pool of cDNA from each treated or infected sample was used to make a 1:10 standard curve with each standard sample diluted 1:5 to produce a linear curve. RT-qPCR was performed using Power-Up SYBR Green Master Mix (Thermo Fisher) using a Quant Studio Flex 6 (Applied Biosystems). Samples were run in triplicate wells in a 96-well or 384 well plate. Averages of the raw values were normalized to average values for the same sample with the control gene, *beta-actin*. To analyze fold induction, the average of the treated sample was divided by the untreated control sample, which was set at 1.

Immunofluorescence Microscopy

Glass coverslips were incubated in 100μl poly-lysine at 37°C for 30 minutes. MEF cells were plated at a density of $2x10^4$ on glass coverslips in 24-well plates and left to grow overnight. Cells were then transfected with 250ng of the desired plasmid(s) using PolyJet. The next day cells were treated with 1μg ISD as described above. At the designated time points, cells were washed with PBS (Thermo Fisher) and then fixed in 4% paraformaldehyde for 10 minutes. Fixed cells were washed three times in PBS and permeabilized by incubating them in PBS containing 5% non-fat milk and 0.05% saponin (Calbiochem). Coverslips were placed in primary antibody for 1 hour then washed 3x in PBS and placed in secondary antibody. These were washed twice in PBS and

twice in deionized water, followed by mounting onto a glass slide using ProLong Diamond antifade mountant (Invitrogen). Images were acquired on a Nikon A1-Confocal Microscope. DAPI nuclear staining (Thermo Fisher).

Co-localization experiments with *M. tuberculosis*

RAW 264.7 macrophages were plated on glass coverslips at a density of $3 \times 10^5$ cells/well in 24-well plates. Cells were infected with m-Cherry *M. tuberculosis* at an MOI of 1 and fixed and stained as above at the designated time points. Colocalization of $\alpha$-TRIM14 G-15 (Santa Cruz sc79761), with *M. tuberculosis* was visualized directly by fluorescence microscopy. A series of images were captured and analyzed by counting the number of bacteria that colocalized with the corresponding marker. At least one hundred events were analyzed per coverslip and each condition was performed with triplicate coverslips.

Protein Expression and Purification

The cDNA encoding mouse TRIM14 (residues 247 to 440), mouse IRF-3 (residues 184-419) were cloned into a modified pET28(a) vector containing an N-terminal Avi-His6-SUMO tag. Sequences of the plasmids were confirmed by DNA sequencing. The BL21 (DE3) cells were co-transformed with the pET28(a) plasmids coding for the target proteins and the pBirAcm plasmid coding for BirA and induced with 0.4 mM IPTG in the presence of 5 μg ml−1 biotin and cultured at 16 °C overnight. The Biotin-labelled-Avi-His6-SUMO proteins were purified using a nickel-NTA column followed by gel-filtration chromatography using a HiLoad 16/60 Superdex 75 column (GE Healthcare). Mouse and human TBK1 (residues 1 to 657) were cloned into the pAcGHLTc baculovirus transfer vector. The plasmid was transfected together with Baculo-Gold bright linearized baculovirus DNA (BD Biosciences) into sf9 insect cells to generate recombinant baculovirus. The original recombinant viruses were amplified for at least two rounds before the large-scale protein expression. The insect cells at a density of $2.5 \times 10^6$ cells/ml were infected by TBK1 recombinant baculovirus and cultured at 27°C and harvested 72 hours post infection. The cells were lysed in the buffer containing 150 mM NaCl, 0.2 M Tris-HCl, 1% NP-40, 1 mM PMSF at pH 8.0. The target protein in the supernatant was purified using nickel affinity chromatography followed by size-exclusion chromatography.

SPR Binding Study

The binding studies between mouse TRIM14 and TBK1 were performed using a Biacore X100 SPR instrument (GE Healthcare). Biotin-labeled SUMO-fusion TRIM14 was coupled on the sensor chip SA (GE Healthcare). Dilution series of TBK1 or IRF-3 (1.25, 2.5, 5, 10, 20 μM) in 1× HBS-EP+ buffer (GE Healthcare) were injected over the sensor chip at a flow rate of 30 μL/min. The single-cycle kinetic/affinity protocol was used in all binding studies. All measurements were

duplicated under the same conditions. The equilibrium $K_d$ was determined by fitting the data to a steady-state 1:1 binding model using Biacore X100 Evaluation software version 2.0 (GE Healthcare).

Chromatin Immunoprecipitation

Chromatin Immunoprecipitation (ChIP) was adapted from Abcam's protocol. Briefly, one confluent 15 cm dish of CRISPR/Cas9 RAW 264.7 macrophages were crosslinked in formaldehyde to a final concentration of 0.75% and rotated for 10 minutes. Glycine was added to stop the cross linking by shaking for 5 minutes at a concentration of 125 mM. Cells were rinsed with PBS twice and then scraped into 5 mL PBS and centrifuged at 1,000g for 5 min at 4C. Cellular pellets were resuspended in ChIP lysis buffer (50 mM HEPES-KOH pH7.5, 140 mM NaCl, 1 mM EDTA pH8, 1% Triton X-100, 0.1% Sodium Deoxycholate, 0.1% SDS Protease Inhibitors) (750 µL per $1\times10^7$ cells) and incubated for 10 min on ice. Cellular lysates were sonicated for 40 minutes (30sec ON, 30sec OFF) on high in a Bioruptor UCD-200 (Diagenode). After sonication, cellular debris was pelleted by centrifugation for 10 min, 4°C, 8,000 × g. Input samples were taken at this step and stored at −80°C until decrosslinking. Approximately 25 µg of DNA diluted to 1:10 with RIPA buffer was used for overnight immunoprecipitation. Each ChIP had one sample for the specific antibody and one sample for Protein G beads only which were pre-blocked for 1 hr with single stranded herring sperm DNA (75 ng/µL) and BSA (0.1 µg/µL). The respective primary antibody was added to all samples except the beads-only sample at a concentration of 5 ug and rotated at 4°C overnight. Beads were washed 3x in with a final wash in high salt (500mM NaCl). DNA was eluted with elution buffer and rotated for 15 min at 30C. Centrifuge for 1 min at 2,000 × g and transfer the supernatant into a fresh tube. Supernatant was incubated in NaCl, RNase A (10 mg/mL) and proteinase K (20 mg/mL) and incubated at 65°C for 1 h. DNA was purified using phenol:chloroform extraction. DNA levels were measure by RT-qPCR. Primers were designed by tiling each respective gene every 500 base pairs that were inputted into NCBI primer design.

mRNA sequencing

RNA was isolated using PureLink RNA mini kits (Ambion) and quantified on a Bioanalyzer 2100 (Agilent). PolyA+ PE 100 libraries were sequenced on a HiSeq 4000 at the UC Davis Genome Center DNA Technologies and Expression Analysis Core. Heatmaps were generated by performing Cluster analysis (Cluster3) followed by Java TreeView. Transcriptome analysis was performed using IPA analysis to generate GO term and disease pathway lists.

VSV infection

RAW 264.7 cells were seeded in 12-well plates at $8\times10^5$ 16h before infection. Cells were infected with VSV-GFP virus at multiplicity of infection (MOI) of 1 in serum-free DMEM (HyClone

SH30022.01). After 1h of incubation with media containing virus, supernatant was removed, and fresh DMEM plus 10% FBS was added to each well. At indicated times post infection, cells were harvested with Trizol and prepared for RNA isolation.

Statistics

Statistical analysis of data was performed using GraphPad Prism software (GraphPad). Two-tailed unpaired Student's t tests were used for statistical analyses, and unless otherwise noted, all results are representative of at least three independent biological experiments and are reported as the mean ± SD (n = 3 per group).

## REFERENCES


1. Underhill, D. M., A. Ozinsky, K. D. Smith, and A. Aderem. 1999. Toll-like receptor-2 mediates mycobacteria-induced proinflammatory signaling in macrophages. *Proc. Natl. Acad. Sci. U.S.A.* 96: 14459–14463.

2. Watson, R. O., S. L. Bell, D. A. MacDuff, J. M. Kimmey, E. J. Diner, J. Olivas, R. E. Vance, C. L. Stallings, H. W. Virgin, and J. S. Cox. 2015. The Cytosolic Sensor cGAS Detects Mycobacterium tuberculosis DNA to Induce Type I Interferons and Activate Autophagy. *Cell Host Microbe* 17: 811–819.

3. Wassermann, R., M. F. Gulen, C. Sala, S. G. Perin, Y. Lou, J. Rybniker, J. L. Schmid-Burgk, T. Schmidt, V. Hornung, S. T. Cole, and A. Ablasser. 2015. Mycobacterium tuberculosis Differentially Activates cGAS- and Inflammasome-Dependent Intracellular Immune Responses through ESX-1. *Cell Host Microbe* 17: 799–810.

4. Collins, A. C., H. Cai, T. Li, L. H. Franco, X.-D. Li, V. R. Nair, C. R. Scharn, C. E. Stamm, B. Levine, Z. J. Chen, and M. U. Shiloh. 2015. Cyclic GMP-AMP Synthase Is an Innate Immune DNA Sensor for Mycobacterium tuberculosis. *Cell Host Microbe* 17: 820–828.

5. Manca, C., L. Tsenova, A. Bergtold, S. Freeman, M. Tovey, J. M. Musser, C. E. Barry, V. H. Freedman, and G. Kaplan. 2001. Virulence of a Mycobacterium tuberculosis clinical isolate in mice is determined by failure to induce Th1 type immunity and is associated with induction of IFN-alpha /beta. *Proc. Natl. Acad. Sci. U.S.A.* 98: 5752–5757.

6. Berry, M. P. R., C. M. Graham, F. W. McNab, Z. Xu, S. A. A. Bloch, T. Oni, K. A. Wilkinson, R. Banchereau, J. Skinner, R. J. Wilkinson, C. Quinn, D. Blankenship, R. Dhawan, J. J. Cush, A. Mejias, O. Ramilo, O. M. Kon, V. Pascual, J. Banchereau, D. Chaussabel, and A. O'Garra. 2010. An interferon-inducible neutrophil-driven blood transcriptional signature in human tuberculosis. *Nature* 466: 973–977.

7. Watson, R. O., P. S. Manzanillo, and J. S. Cox. 2012. Extracellular M. tuberculosis DNA targets bacteria for autophagy by activating the host DNA-sensing pathway. *Cell* 150: 803–815.

8. van Gent, M., K. M. J. Sparrer, and M. U. Gack. 2018. TRIM Proteins and Their Roles in Antiviral Host Defenses. *Annu Rev Virol* 5: 385–405.

9. Rajsbaum, R., A. García-Sastre, and G. A. Versteeg. 2014. TRIMmunity: the roles of the TRIM E3-ubiquitin ligase family in innate antiviral immunity. *J. Mol. Biol.* 426: 1265–1284.

10. Versteeg, G. A., R. Rajsbaum, M. T. Sánchez-Aparicio, A. M. Maestre, J. Valdiviezo, M. Shi, K.-S. Inn, A. Fernandez-Sesma, J. Jung, and A. García-Sastre. 2013. The E3-ligase TRIM family of proteins regulates signaling pathways triggered by innate immune pattern-recognition receptors. *Immunity* 38: 384–398.

11. Koliopoulos, M. G., D. Esposito, E. Christodoulou, I. A. Taylor, and K. Rittinger. 2016. Functional role of TRIM E3 ligase oligomerization and regulation of catalytic activity. *EMBO J.* 35: 1204–1218.

12. Sanchez, J. G., K. Okreglicka, V. Chandrasekaran, J. M. Welker, W. I. Sundquist, and O. Pornillos. 2014. The tripartite motif coiled-coil is an elongated antiparallel hairpin dimer. *Proc. Natl. Acad. Sci. U.S.A.* 111: 2494–2499.

13. Stremlau, M., C. M. Owens, M. J. Perron, M. Kiessling, P. Autissier, and J. Sodroski. 2004. The cytoplasmic body component TRIM5alpha restricts HIV-1 infection in Old World monkeys. *Nature* 427: 848–853.

14. Lang, X., T. Tang, T. Jin, C. Ding, R. Zhou, and W. Jiang. 2017. TRIM65-catalized ubiquitination is essential for MDA5-mediated antiviral innate immunity. *J. Exp. Med.* 214: 459–473.

15. Sanchez, J. G., J. J. Chiang, K. M. J. Sparrer, S. L. Alam, M. Chi, M. D. Roganowicz, B. Sankaran, M. U. Gack, and O. Pornillos. 2016. Mechanism of TRIM25 Catalytic Activation in the Antiviral RIG-I Pathway. *Cell Rep* 16: 1315–1325.

16. Zhao, C., M. Jia, H. Song, Z. Yu, W. Wang, Q. Li, L. Zhang, W. Zhao, and X. Cao. 2017. The E3 Ubiquitin Ligase TRIM40 Attenuates Antiviral Immune Responses by Targeting MDA5 and RIG-I. *Cell Rep* 21: 1613–1623.

17. Narayan, K., L. Waggoner, S. T. Pham, G. L. Hendricks, S. N. Waggoner, J. Conlon, J. P. Wang, K. A. Fitzgerald, and J. Kang. 2014. TRIM13 is a negative regulator of MDA5-mediated type I interferon production. *J. Virol.* 88: 10748–10757.

18. Sparrer, K. M. J., S. Gableske, M. A. Zurenski, Z. M. Parker, F. Full, G. J. Baumgart, J. Kato, G. Pacheco-Rodriguez, C. Liang, O. Pornillos, J. Moss, M. Vaughan, and M. U. Gack. 2017. TRIM23 mediates virus-induced autophagy via activation of TBK1. *Nat Microbiol* 2: 1543–1557.
19. Porritt, R. A., and P. J. Hertzog. 2015. Dynamic control of type I IFN signalling by an integrated network of negative regulators. *Trends Immunol.* 36: 150–160.
20. Patrick, K. L., S. L. Bell, and R. O. Watson. 2016. For Better or Worse: Cytosolic DNA Sensing during Intracellular Bacterial Infection Induces Potent Innate Immune Responses. *J. Mol. Biol.* 428: 3372–3386.
21. Zhang, Y., L. Yeruva, A. Marinov, D. Prantner, P. B. Wyrick, V. Lupashin, and U. M. Nagarajan. 2014. The DNA sensor, cyclic GMP-AMP synthase, is essential for induction of IFN-β during Chlamydia trachomatis infection. *J. Immunol.* 193: 2394–2404.
22. Woodward, J. J., A. T. Iavarone, and D. A. Portnoy. 2010. c-di-AMP secreted by intracellular Listeria monocytogenes activates a host type I interferon response. *Science* 328: 1703–1705.
23. Fiskin, E., S. Bhogaraju, L. Herhaus, S. Kalayil, M. Hahn, and I. Dikic. 2017. Structural basis for the recognition and degradation of host TRIM proteins by Salmonella effector SopA. *Nat Commun* 8: 14004–14.
24. Kamanova, J., H. Sun, M. Lara-Tejero, and J. E. Galán. 2016. The Salmonella Effector Protein SopA Modulates Innate Immune Responses by Targeting TRIM E3 Ligase Family Members. *PLoS Pathog.* 12: e1005552.
25. Ye, W., M.-M. Hu, C.-Q. Lei, Q. Zhou, H. Lin, M.-S. Sun, and H.-B. Shu. 2017. TRIM8 Negatively Regulates TLR3/4-Mediated Innate Immune Response by Blocking TRIF-TBK1 Interaction. *J. Immunol.* 199: 1856–1864.
26. Nagre, N., X. Cong, H.-L. Ji, J. M. Schreiber, H. Fu, I. Pepper, S. Warren, J. M. Sill, R. D. Hubmayr, and X. Zhao. 2018. Inhaled TRIM72 Protein Protects Ventilation Injury to the Lung through Injury-guided Cell Repair. *Am. J. Respir. Cell Mol. Biol.* 59: 635–647.
27. Wu, X., J. Wang, S. Wang, F. Wu, Z. Chen, C. Li, G. Cheng, and F. X.-F. Qin. 2019. Inhibition of Influenza A Virus Replication by TRIM14 via Its Multifaceted Protein-Protein Interaction With NP. *Front Microbiol* 10: 344.
28. Tan, G., F. Xu, H. Song, Y. Yuan, Q. Xiao, F. Ma, F. X.-F. Qin, and G. Cheng. 2018. Identification of TRIM14 as a Type I IFN-Stimulated Gene Controlling Hepatitis B Virus Replication by Targeting HBx. *Front Immunol* 9: 1872.
29. Wang, S., Y. Chen, C. Li, Y. Wu, L. Guo, C. Peng, Y. Huang, G. Cheng, and F. X.-F. Qin. 2016. TRIM14 inhibits hepatitis C virus infection by SPRY domain-dependent targeted degradation of the viral NS5A protein. *Sci Rep* 6: 32336–12.
30. Zhou, Z., X. Jia, Q. Xue, Z. Dou, Y. Ma, Z. Zhao, Z. Jiang, B. He, Q. Jin, and J. Wang. 2014. TRIM14 is a mitochondrial adaptor that facilitates retinoic acid-inducible gene-I-like receptor-mediated innate immune response. *Proc. Natl. Acad. Sci. U.S.A.* 111: E245–54.
31. Chen, M., Q. Meng, Y. Qin, P. Liang, P. Tan, L. He, Y. Zhou, Y. Chen, J. Huang, R.-F. Wang, and J. Cui. 2016. TRIM14 Inhibits cGAS Degradation Mediated by Selective Autophagy Receptor p62 to Promote Innate Immune Responses. *Mol. Cell* 64: 105–119.
32. Stanley, S. A., J. E. Johndrow, P. Manzanillo, and J. S. Cox. 2007. The Type I IFN response to infection with Mycobacterium tuberculosis requires ESX-1-mediated secretion and contributes to pathogenesis. *J. Immunol.* 178: 3143–3152.
33. Manzanillo, P. S., M. U. Shiloh, D. A. Portnoy, and J. S. Cox. 2012. Mycobacterium tuberculosis activates the DNA-dependent cytosolic surveillance pathway within macrophages. *Cell Host Microbe* 11: 469–480.
34. Schoggins, J. W., D. A. MacDuff, N. Imanaka, M. D. Gainey, B. Shrestha, J. L. Eitson, K. B. Mar, R. B. Richardson, A. V. Ratushny, V. Litvak, R. Dabelic, B. Manicassamy, J. D. Aitchison, A. Aderem, R. M. Elliott, A. García-Sastre, V. Racaniello, E. J. Snijder, W. M. Yokoyama, M. S. Diamond, H. W. Virgin, and C. M. Rice. 2014. Pan-viral specificity of IFN-induced genes reveals new roles for cGAS in innate immunity. *Nature* 505: 691–695.
35. Stetson, D. B., and R. Medzhitov. 2006. Recognition of cytosolic DNA activates an IRF3-dependent innate immune response. *Immunity* 24: 93–103.
36. Li, X., C. Shu, G. Yi, C. T. Chaton, C. L. Shelton, J. Diao, X. Zuo, C. C. Kao, A. B. Herr, and P. Li. 2013. Cyclic GMP-AMP synthase is activated by double-stranded DNA-induced oligomerization. *Immunity* 39: 1019–1031.

37. Shu, C., B. Sankaran, C. T. Chaton, A. B. Herr, A. Mishra, J. Peng, and P. Li. 2013. Structural insights into the functions of TBK1 in innate antimicrobial immunity. *Structure* 21: 1137–1148.
38. Larabi, A., J. M. Devos, S.-L. Ng, M. H. Nanao, A. Round, T. Maniatis, and D. Panne. 2013. Crystal structure and mechanism of activation of TANK-binding kinase 1. *Cell Rep* 3: 734–746.
39. Hemmi, H., O. Takeuchi, S. Sato, M. Yamamoto, T. Kaisho, H. Sanjo, T. Kawai, K. Hoshino, K. Takeda, and S. Akira. 2004. The roles of two IkappaB kinase-related kinases in lipopolysaccharide and double stranded RNA signaling and viral infection. *J. Exp. Med.* 199: 1641–1650.
40. Perry, A. K., E. K. Chow, J. B. Goodnough, W.-C. Yeh, and G. Cheng. 2004. Differential requirement for TANK-binding kinase-1 in type I interferon responses to toll-like receptor activation and viral infection. *J. Exp. Med.* 199: 1651–1658.
41. Fitzgerald, K. A., S. M. McWhirter, K. L. Faia, D. C. Rowe, E. Latz, D. T. Golenbock, A. J. Coyle, S.-M. Liao, and T. Maniatis. 2003. IKKepsilon and TBK1 are essential components of the IRF3 signaling pathway. *Nat. Immunol.* 4: 491–496.
42. Tanaka, Y., and Z. J. Chen. 2012. STING specifies IRF3 phosphorylation by TBK1 in the cytosolic DNA signaling pathway. *Sci Signal* 5: ra20–ra20.
43. Wang, W.-B., D. E. Levy, and C.-K. Lee. 2011. STAT3 negatively regulates type I IFN-mediated antiviral response. *J. Immunol.* 187: 2578–2585.
44. Tsai, M.-H., L.-M. Pai, and C.-K. Lee. 2019. Fine-Tuning of Type I Interferon Response by STAT3. *Front Immunol* 10: 1448.
45. Hsia, H.-C., J. E. Hutti, and A. S. Baldwin. 2017. Cytosolic DNA Promotes Signal Transducer and Activator of Transcription 3 (STAT3) Phosphorylation by TANK-binding Kinase 1 (TBK1) to Restrain STAT3 Activity. *J. Biol. Chem.* 292: 5405–5417.
46. Ivashkiv, L. B., and L. T. Donlin. 2014. Regulation of type I interferon responses. *Nat. Rev. Immunol.* 14: 36–49.
47. Honke, N., N. Shaabani, D.-E. Zhang, C. Hardt, and K. S. Lang. 2016. Multiple functions of USP18. *Cell Death Dis* 7: e2444–e2444.
48. Hutchins, A. P., D. Diez, Y. Takahashi, S. Ahmad, R. Jauch, M. L. Tremblay, and D. Miranda-Saavedra. 2013. Distinct transcriptional regulatory modules underlie STAT3's cell type-independent and cell type-specific functions. *Nucleic Acids Res.* 41: 2155–2170.
49. Ramadoss, P., N. E. Unger-Smith, F. S. Lam, and A. N. Hollenberg. 2009. STAT3 targets the regulatory regions of gluconeogenic genes in vivo. *Mol. Endocrinol.* 23: 827–837.
50. Penn, B. H., Z. Netter, J. R. Johnson, J. von Dollen, G. M. Jang, T. Johnson, Y. M. Ohol, C. Maher, S. L. Bell, K. Geiger, G. Golovkine, X. Du, A. Choi, T. Parry, B. C. Mohapatra, M. D. Storck, H. Band, C. Chen, S. Jäger, M. Shales, D. A. Portnoy, R. Hernandez, L. Coscoy, J. S. Cox, and N. J. Krogan. 2018. An Mtb-Human Protein-Protein Interaction Map Identifies a Switch between Host Antiviral and Antibacterial Responses. *Mol. Cell* 71: 637–648.e5.
51. Zhuang, S. 2013. Regulation of STAT signaling by acetylation. *Cell. Signal.* 25: 1924–1931.
52. Wang, R., P. Cherukuri, and J. Luo. 2005. Activation of Stat3 sequence-specific DNA binding and transcription by p300/CREB-binding protein-mediated acetylation. *J. Biol. Chem.* 280: 11528–11534.
53. Jia, X., H. Zhou, C. Wu, Q. Wu, S. Ma, C. Wei, Y. Cao, J. Song, H. Zhong, Z. Zhou, and J. Wang. 2017. The Ubiquitin Ligase RNF125 Targets Innate Immune Adaptor Protein TRIM14 for Ubiquitination and Degradation. *J. Immunol.* 198: 4652–4658.
54. Kim, B.-H., A. R. Shenoy, P. Kumar, R. Das, S. Tiwari, and J. D. MacMicking. 2011. A family of IFN-γ-inducible 65-kD GTPases protects against bacterial infection. *Science* 332: 717–721.

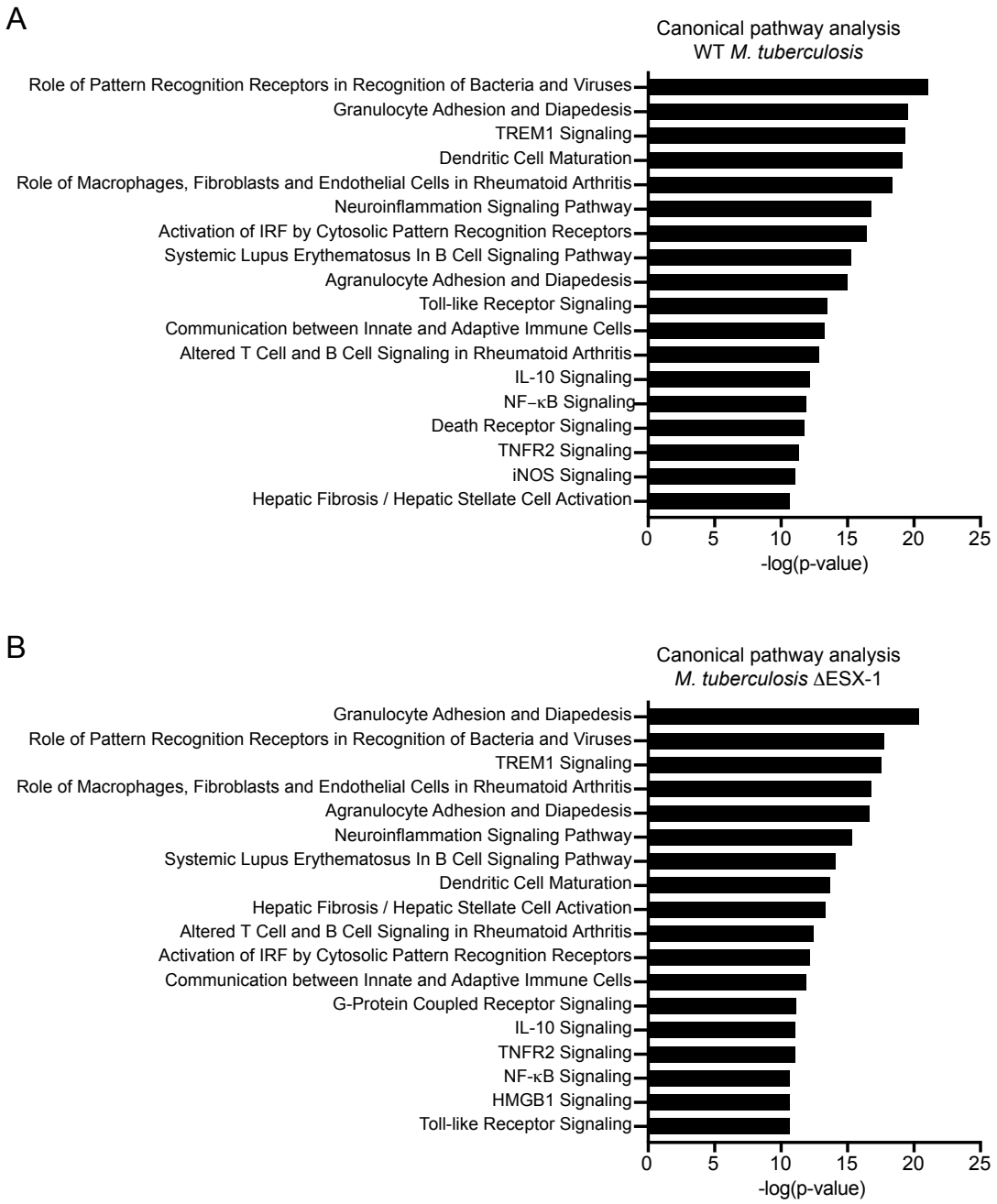


**Figure S1.** (A) IPA software analysis of cellular pathways enriched for differentially expressed genes in BMDMs infected with WT *M. tuberculosis***.** (B) IPA software analysis of cellular pathways enriched for differentially expressed genes in BMDMs infected with ΔESX-1 *M. tuberculosis***.**

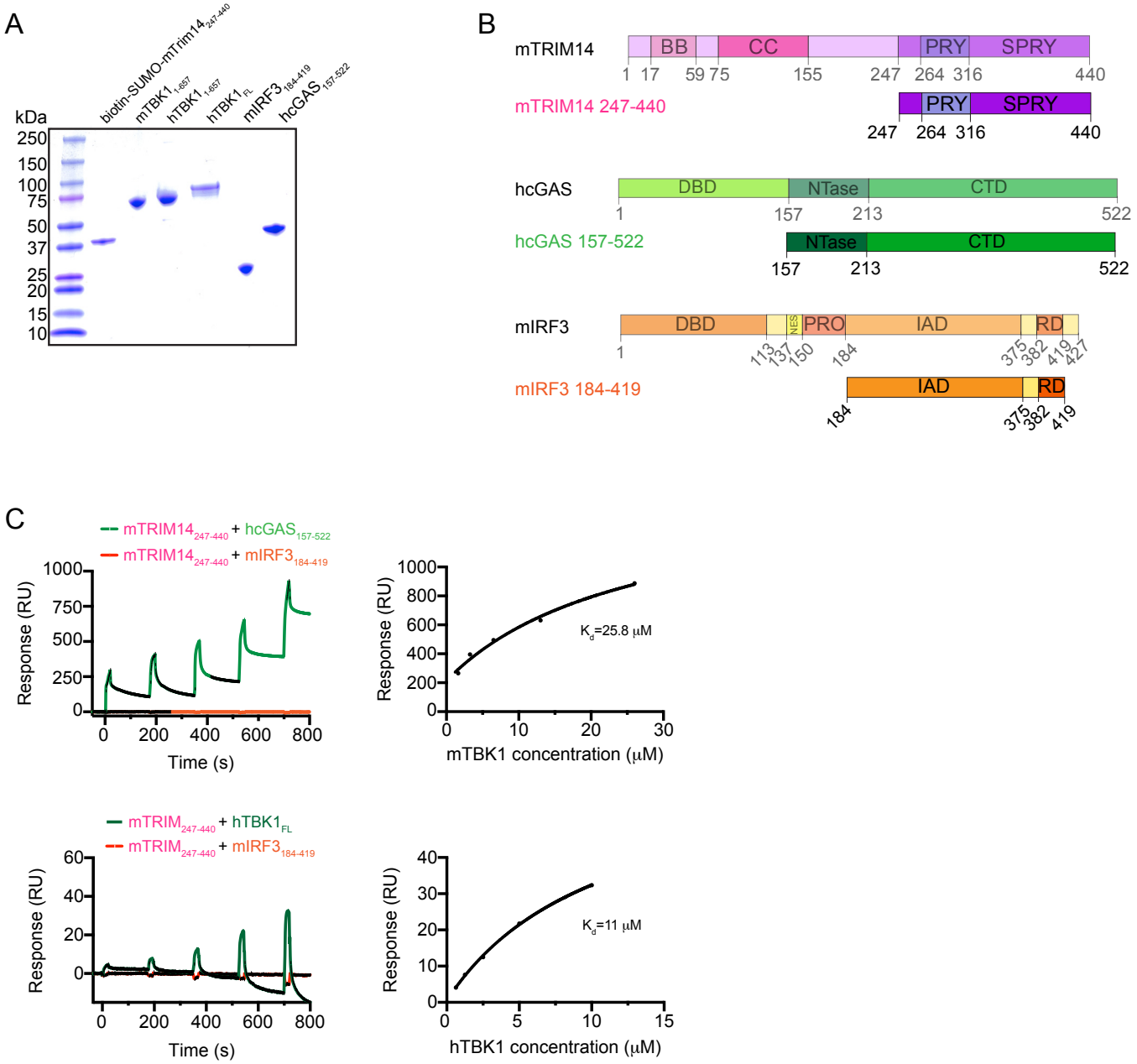


**Figure S2.** (A) Protein expression of mTRIM14, mTBK1, hTBK1, mIRF3, and hcGAS. (B) Diagram of mTRIM14, mIRF3, and hcGAS gene domains and truncations used in SPR studies. (C) Equilibrium binding study of mTRIM14 and hcGAS by surface plasmon resonance (SPR). mIRF3 was used as a negative control. Dissociation constant ($K_d$= 25.8 μM) was derived by fitting of the equilibrium binding data to a one-site binding model. Equilibrium binding study of mTRIM14 and hTBK1 by surface plasmon resonance (SPR). mIRF3 was used as a negative control. Dissociation constant ($K_d$= 11 μM) was derived by fitting of the equilibrium binding data to a one-site binding model.

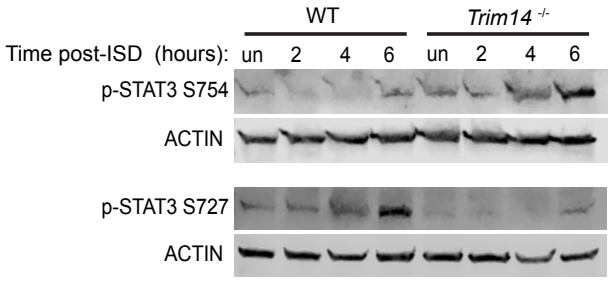


**Figure S5.** Immunoblot of phospho-STAT3 Ser754, phospho-STAT3 Ser727, and phospho-STAT1 Y701 in WT and *Trim14* KO RAW 264.7 macrophages at 1, 2, 4, 6, 8h post recombinant IFNb treatment. ACTIN is shown as a loading control.

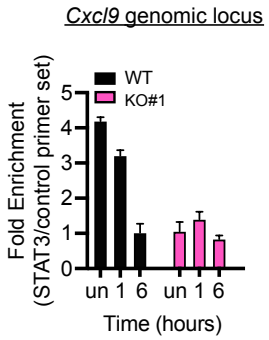


**Figure S6.** ChIP-qPCR of 3xFLAG-STAT3 associated genomic DNA from the CXCL9 locus in WT and *Trim14* KO RAW 264.7 macrophages transfected with 1 μg ISD.

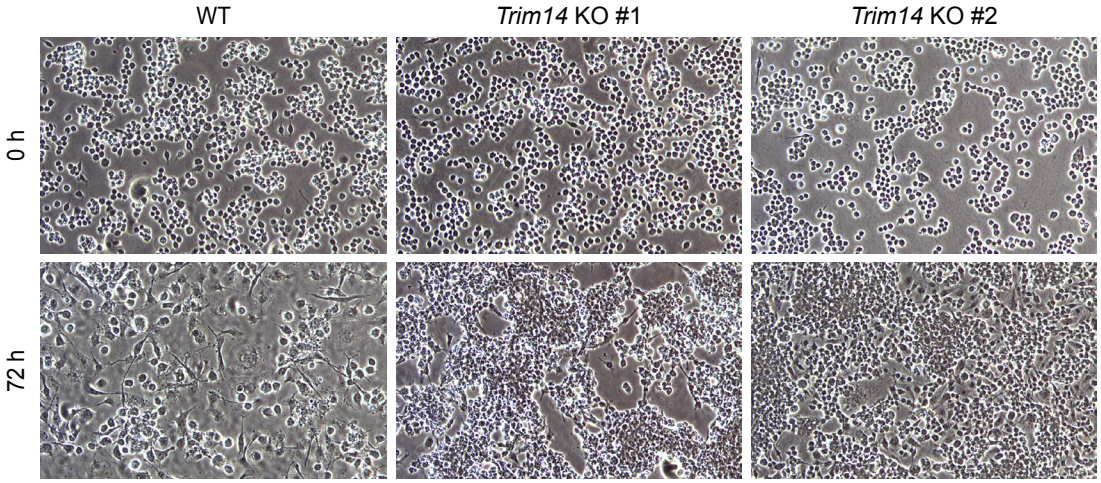


**Figure S7.** Phase contrast images showing monolayers of WT and *Trim14* KO RAW 264.7 macrophages infected with Mtb *luxBCADE*.